WIND TURBINE WAKES AND WIND FARM WAKES

REPORT 2018:541

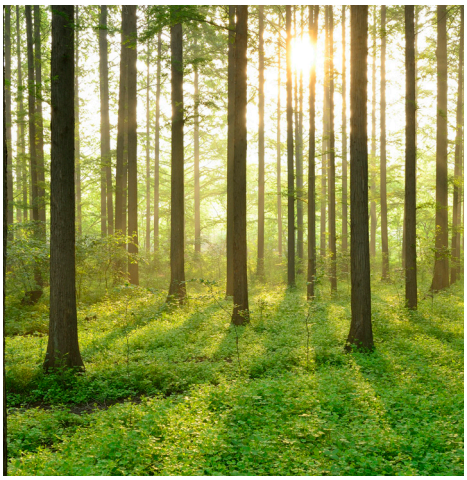

VINDFORSK

Energiforsk

Wind Turbine Wakes and Wind Farm Wakes

– what are todays model possibilities and accuracy?

STEFAN IVANELL, KARL NILSSON, OLA ERIKSSON,
STEFAN SÖDERBERG OCH INGEMAR CARLÉN

ISBN 978-91-7673-541-1 | © Energiforsk November 2018

Energiforsk AB | Phone: 08-677 25 30 | E-mail: kontakt@energiforsk.se | www.energiforsk.se

Foreword

Projektet "Wind turbine wakes and wind farm wakes" har finansierats av Energiforsk och Energimyndigheten genom programmet Vindforsk IV.

Syftet har varit att utveckla metoder för att öka kunskapen om hur vindvakar påverkar omgivande vindkraftverk, såväl inom en park som mellan parker. Målet har varit att utveckla verktyg för att optimera utformningen av större vindparker och för att minska lasterna på vindkraftverken.

Mikroskalesimuleringar har gjorts av befintliga vindkraftparker med goda resultat liksom mesoskalesimuleringar för att undersöka påverkan mellan stora vindkraftsanläggningar till havs.

Med tanke på kommande etablering av mycket stora vindkraftparker, främst till havs, är forskningsområdet av stor vikt för framtida utbyggnad av vindkraft.

Projektet har genomförts i en internationell samverkan och öppnat upp för kommande samarbete. Projektet har genomförts av Stefan Ivanell, projektledare, Uppsala Universitet tillsammans med Karl Nilsson och Ola Eriksson från Uppsala universitet, Stefan Söderberg från Weathertech Scandinavia och Ingemar Carlén från Teknikgruppen.

Göran Dalén

Ordförande, Vindforsk IV

Sammanfattning

När ett vindkraftverk tar tillvara vindens rörelseenergi skapas en vak bakom det som kännetecknas av lägre vindhastighet och ökad turbulens. Jämfört med enstaka vindkraftverk så minskar produktionen och lastpåverkan ökar vid placering av vindkraftverk i grupper och vid placering av flera vindkraftparker i närheten av varandra.

Målet med projektet var att göra framsteg i möjligheter att modellera vindkraftparker och interaktion mellan parker. Att ytterligare öka kunskapen om begränsningarna för olika simuleringsmetoder var ett ytterligare mål. Genom ökade möjligheter att uppskatta påverkan av vakar så kan mer optimal placering av vindkraftverk i grupper samt mer optimal drift uppnås.

Mikroskalesimuleringar genomfördes av Uppsala universitet och mesoskalesimuleringar genomfördes av WeatherTech Scandinavia. Vattenfall bidrog med industriell erfarenhet samt data. Data från vindkraftparken Lillgrund användes för utvärdering av lastpåverkan av Teknikgruppen. Data från vindkraftparkerna Lillgrund samt Horns Rev användes för jämförelse med simuleringsresultat.

Mikroskalemetoden har visats både i denna och tidigare studier ha tillräcklig noggrannhet. Ytterligare utveckling och utvärdering av metoden (LES simuleringar och Actuator disk) för användning för studier av vindkraftparker liksom flödet bakom dessa gjordes inom projektet.

Vi kan simulera produktionen inom stora vindkraftparker med en så kallad Actuator disk metod. Ett exempel är parksimuleringar av Lillgrund som visade utmärkt överenstämmelse med mätningar.

Den använda mikroskalemetoden kan användas för studier av vakar bakom hela vindkraftparker även om det kräver stor beräkningskapacitet. För studier av park-park interaktionsfall så är beräkningskapacitetsbehovet i dagsläget för stort. En mesoskalemetod inkluderar fler meteorologiska parametrar och har ett lägre beräkningskapacitetsbehov. Den behöver dock också parameterisera vindkraftverken och ger därmed färre detaljer inom vindkraftparken. För att inkludera all den fysik som krävs för studier av park-park interaktion är en lösning att utarbeta en metodik för att kunna kombinera dessa metoder.

En utmaning för simuleringar är att en kompromiss görs mellan beräkningsnoggrannhet och beräkningskapacitetsbehov. Den använda mikroskalemetoden är för beräkningstung för industrin men genom att genomföra denna typ av simuleringar i forskningsgrupper kan dessa visa vägen framåt och metoden kan användas för validering av ingenjörsmodeller.

För att i framtiden kunna modellera såväl detaljer som olika atmosfäriska tillstånd krävs ytterligare utveckling av simuleringsmetoden. Inom projektet har dock stora steg tagits i den riktningen.

Summary

A wind turbine that extracts kinetic energy from the wind will result in a wind turbine wake behind it characterized by reduced wind speed and increased turbulence. Placing wind turbines in wind farms and wind farms in clusters will result in less production and increased loads compared to single turbines.

The aim with this project has been to make advancements in the possibilities of how to model farms and interaction of farms. In addition, the aim was to increase knowledge about limitations in different modeling methodologies. With better possibilities to assess these interactions more optimized placement of wind turbines and operations can be achieved.

State-of-art microscale modeling was performed by Uppsala University and mesoscale modelling was performed by WeatherTech Scandinavia. Vattenfall contributed with industrial experiences and data. Data from the Lillgrund wind farm was used for load assessment by Teknikgruppen. Data from the wind farms of Lillgrund and Horns Rev was also used for comparison with modelling results.

The microscale methodology has been verified to work with satisfactory accuracy within this and other studies. Further development and evaluation of the model (LES simulations and an actuator disc method) for studies of wind farms as well as the flow behind it was performed in the project.

We are able to simulate the power production inside large wind farms using so called actuator disc methodology. For example, the farm simulations of Lillgrund shows excellent agreement with measurements.

The used Microscale model can be used for studies of long distance wakes behind wind farms but the computational effort is high. For farm to farm interaction cases the computational demand is at the moment too high. A mesoscale model includes more meteorological parameters and is also less computational demanding although a wind turbine parameterization is needed which gives less details of the flow inside the wind farms. Therefore, we need capabilities from both methodologies to be able to fully model the physics for farm-farm interaction and to couple these methodologies is a solution to further develop.

A challenge for modelling is that there is a compromise between accuracy and required computational time. The used microscale method would be too computational demanding for industry but by performing this type of simulation in research groups we can show the way and also use these simulations as verification to engineering models.

Future work is needed to further develop the simulation methodology to be able to model details as well as atmospheric conditions in the future. This project has, however, made large steps in that direction.

List of content

1 Introduction

1.1 THE WIND TURBINE WAKE

According to the well-known Betz limit (Betz 1920) no more than approximately 59.3% (16/27) of the kinetic energy in the wind can be extracted and transformed into rotational energy by the rotor. This means that the turbine extracts momentum from the flow leading to lower kinetic energy in the wake flow, and thus a lower mean velocity, compared to the undisturbed flow upstream of the turbine. Furthermore, as the turbine blades sweep the air, each blade induces a vortex sheet which transforms into tip and root vortices behind the turbine. Since the blades are rotating, these vortices create helical structures as seen in Figure 1-1. These structures will eventually break down into smaller scale turbulence due to different instability mechanisms such as the vortex pairing of the tip vortices (Sarmast et al. 2014) as depicted in Figure 1-1. This figure is generated by a large-eddy simulation (LES) in which the turbine is modeled using the so-called actuator line (ACL) method.

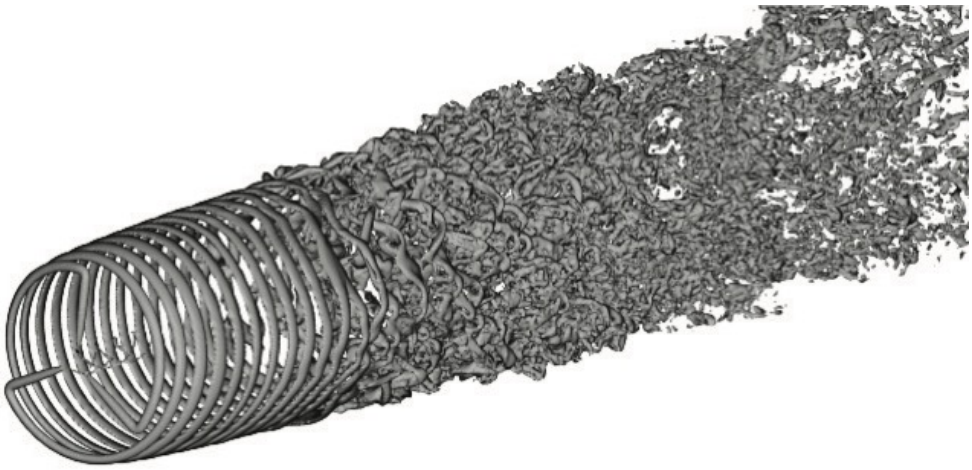

Figure 1-1: The vortex structure behind a wind turbine.

The wake behind a wind turbine is characterized by two regions; the near and the far wake. The near wake is the region in the vicinity of the turbine where the wake features are directly linked to the rotor geometry and its aerodynamics as well as to the inflow conditions. The near wake is characterized by the helical vortex structures described above which gradually undergoes a transition into smaller scale turbulence. The near wake is followed by the far wake in which the influence of the rotor characteristics is less important. The far wake is more influenced by the surrounding environment, such as wakes from other turbines and the topography. In the far wake the cross-sectional profiles of velocity and turbulence intensity have self-similar distributions (Vermeer et al. 2003).

Considering that we today are erecting wind turbines in clusters, i.e., the wakes from the individual turbines combines to a farm wake that stretches 10th of kilometers and thus effect, not only downstream turbines but, entire wind farms.

In order to capture all the physics of the wake flow, immense computational power is required. Thus, depending on the problem to be solved, different reduced order models must be used.

1.2 MICRO- AND MESOSCALE MODELS

The simulations in this report are denoted as either microscale or mesoscale. This project scope over a complex challenge due to the fact that the investigated scales scopes over many orders of magnitude, i.e., from turbine scale (order of 0.1 kilometer) to farm scale (order of kilometers) to farm interaction scale (order of 10's of kilometers). The mesoscale (scales above 1 km) simulations are taking most of the atmospheric conditions into account and are covering large domains. Grid resolution is typically coarse which leads to a need for parameterization of small scale phenomena. Since grid cells normally contains several wind turbines, the rotor modeling (similar to the constantly loaded ACD) is a (described more in detail in Section 2.2.1) aggregated value of all the turbines in the cell. Consequently, individual turbine wakes cannot be assessed and the wake flow becomes rather crude.

The microscale (scales below 1 km) simulations are covering smaller domains and, from an atmospheric flow perspective, are only taking the boundary layer and resulting turbulence into account. The grid resolution is high with several grid points dedicated for each wind turbine (typically modelled with any of the actuator models described above). These simulations are therefore suitable for the assessment of individual turbines with a good detail of the resulting wake flows. However, due to the microscale model ability, the atmospheric conditions are normally considered be neutral which is a large simplification to the actually complexity of the atmosphere.

In the New European Wind Atlas project (NEWA, 2018) leading European researchers are joining forces to couple mesoscale and microscale models to gain the benefits and circumvent the drawbacks of the different models.

There are different types of microscale models which are normally divided into linear models, such as WindPRO (EMD, 2018) and WAsP (Risø, 2018), and non-linear, or Computational Fluid Dynamics (CFD) models, such as WindSim and EllipSys3D (see description in Section 2.1). The linear models are not suitable for detailed wake studies due to limitations in their representation of the flow physics. Hence, this report will focus on the usage of CFD models. For wind assessment purposes two different types of CFD models are computationally affordable; Reynolds Averaged Navier-Stokes (RANS) and LES. Réthoré (2009) performed different RANS simulations using an ACD method. The results were compared with LES and measurements. This work showed that LES and measurements were in good agreement and that all of the simulations using the RANS model had problems capturing the full extent of the wake flow. Therefore, the work conducted in the microscale part of this report was using LES.

It should also be mentioned that the mesoscale simulations performed within the current work are also based on a CFD model.

1.3 WAKE MODELS

1.3.1 Engineering models

So-called engineering models are commonly used by the industry. The main reason for this is that these models are highly time efficient and run on normal computers. They are come already implemented in widely used commercial microscale models such as WindPRO, WAsP and WindSim. On the downside, these models generally have a poor representation of the true physics of the wake flow. One example is the Jensen model (Jensen, 1983). This model is based on a simple momentum balance and assumes a linearly expanding wake. The expansion rate should be set to take ambient conditions (such as turbulence) into account. Additionally, this model is a pure far wake model. A true wake flow does not show a linear expansion behavior which is why it comes clear that the Jensen model is largely simplified. For more detailed studies of wake flows, this model is not an option.

1.3.2 Actuator models

Actuator models are used in computational fluid dynamics as a part of the solution to the governing equations. As a result, these models require significantly more time and computational capacity compared to the engineering models. Consequently, the physics of the wake flow is far better captured in the actuator models.

The lowest order actuator model is the actuator disc (ACD) with constant loading. This model is based on the thrust of the turbine and is therefore to be considered as a momentum sink rather than a real turbine. Thrust is normally known for different wind turbines and this model is normally used when more detailed is unavailable. The wake rotation and tip vortex structure are not present in this model. Consequently, the model is not suitable to be used for predicting the near region but is well capable of modeling the far region of the wake flow.

The next level of order is the ACD based on airfoil data (described in more detail in Section 2.1.1). In this case the forces representing the blades are determined from tabulated airfoil data. The power production is determined from the tangential loading, making this approach close to a real turbine. Wake rotation is induced; however, the tip vortex structure is not present in this model. The near wake prediction of this model is therefore better compared to the constantly loaded disc. This model works very well (see Nilsson et al. 2015a for further information) for detailed studies of the effects of wake interaction between several turbines. In Figure 1-2 wakes in the Lillgrund wind farm modeled with the ACD based on airfoil data are depicted.

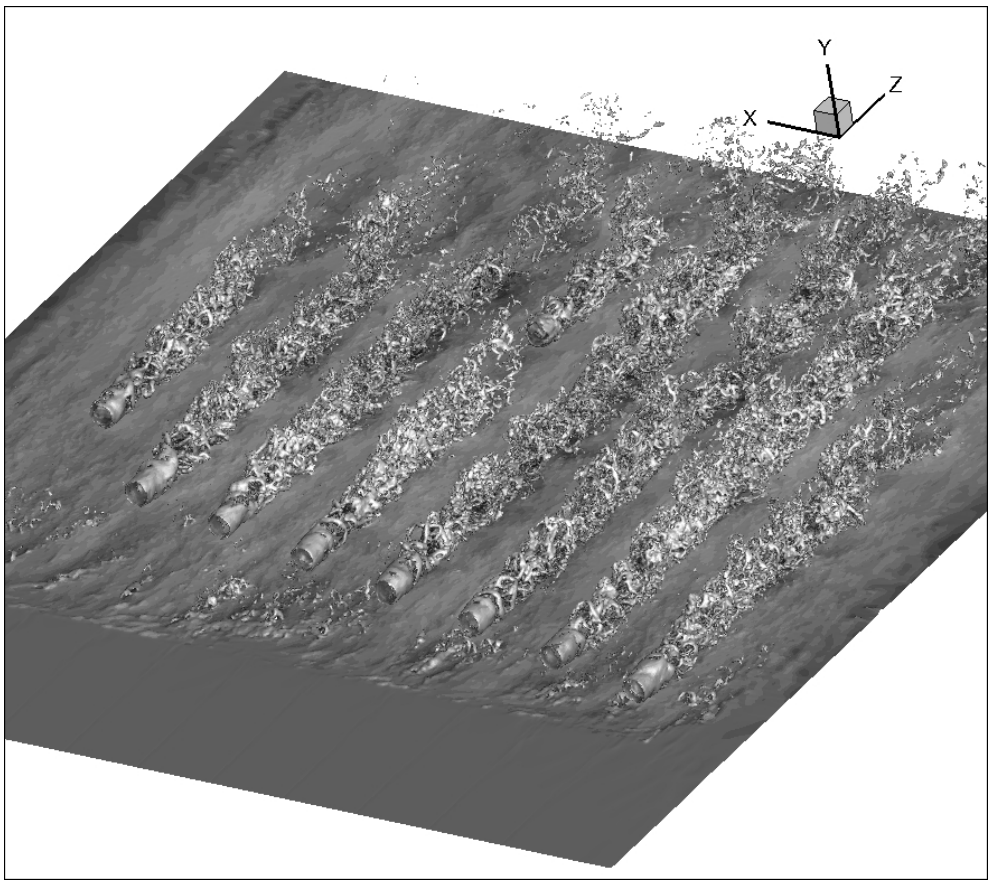

Figure 1-2: Wake visualization of the Lillgrund wind farm.

The next level of model is the ACL model. This model is similar to the ACD model based on airfoil data, with the difference that the turbine blades are modeled with rotating lines instead of a disc. This model dramatically increases the computational demand since the time scales are dependent on the rotational speed of the blades rather than the incoming wind speed and since a much higher resolution is required. However, this model is very close to a real turbine. It predicts the entire chain of the wake flow and corresponds well to measurements (see Nilsson et al. 2015b for further information). Due to the large computational demands this model is restricted to the study of a small number of turbines and is hence not ideal for larger farms.

1.4 AIM AND STRUCTURE OF THE REPORT

This project did include partners from Uppsala University (UU), WeatherTech Scandinavia (WT), Teknikgruppen (TG) and Vattenfall (VF). With these partners we did combine competences in state-of-art microscale modeling (by UU), industrial research front in mesoscale modeling (by WT), long engineering experience of wind turbine and load assessment (by TG) and industrial experiences, data, and identification of knowledge gaps (VF).

The aim with this project has been to make advancements in the possibilities of how to model farms and interaction of farms. In addition, the aim was to increase knowledge about limitations in different modeling methodologies.

The work mainly contains contributions from the following parts;

1. PhD projects focusing on farm scale
2. PhD project focusing on farm to farm scale
3. Contribution from WT in collaboration with the second PhD project also focusing on farm to farm scale.
4. Contribution from VF in farm and farm to farm scale through data sharing, exchange of knowledge and supervision of thesis work in the area.
5. Contribution from TG that have made a detailed database and report on available data from measurements at the Lillgrund wind farm that has partly been used in the current project but also gives an important contribution for follow up projects.

Results from part 1 are described in chapter 3.1-3.3 and 5.1. Results from part 2 are described in chapter 3.3-3.4 and 6. Results from part 3 are described in chapter 5.2 and 6. Contributions from part 4 are included in chapter 3 to 6. The contribution from point 5 is described in a summary in chapter 4. The full report is under NDA conditions and can therefore not be distributed here but the data will be very useful in future projects.

2 Modelling methods

2.1 MICROSCALE MODEL DESCRIPTION

Resolving all length and time scales associated with wind turbines is not possible with today's computational capabilities. Therefore, in this work the approach of LES is used in combination with the actuator disc method.

The simulations are performed with the EllipSys3D code, originally developed by Michelsen (1992, 1994) and Sørensen (1995) at DTU/Risø. The EllipSys3D code is a general purpose 3D solver based on a finite volume discretization of the Navier-Stokes equations. However, in this study all simulations are carried out as LES. This basically means that the large turbulence scales are resolved and the smaller scales are modelled. The following Equation is solved by EllipSys3D:

$$\frac{\partial \overline{\boldsymbol{U}}}{\partial t} + \overline{\boldsymbol{U}} \cdot \nabla \overline{\boldsymbol{U}} = -\frac{1}{\rho}\nabla \overline{\boldsymbol{P}} + \nabla[(\upsilon + \upsilon_{SGS})\nabla \overline{\boldsymbol{U}}] + \frac{1}{\rho}\boldsymbol{f}'_{WTG} + \frac{1}{\rho}\boldsymbol{f}'_{PBL} + \frac{1}{\rho}\boldsymbol{f}'_{turb}$$

The small-scale modelling is introduced in the υ_{SGS} term. The last three parts of the equation are used for the introduction of turbines, a boundary layer and atmospheric turbulence into the equation (see the forthcoming section for further descriptions). Figure 2-1 shows schematically how it works.

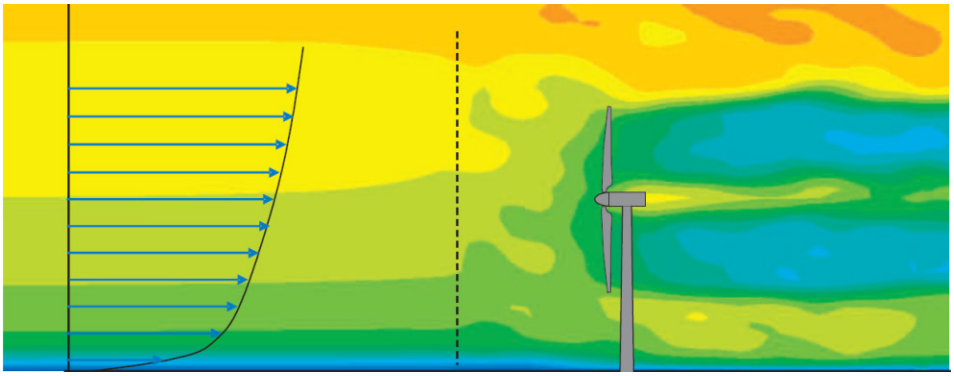

Figure 2-1: The principes of the numerical model.

2.1.1 Turbine model

The turbines are modelled using the ACD method. In the ACD method (Mikkelsen, 2003; Sørensen & Myken, 1992) the blades are represented by body forces ($\boldsymbol{f}'_{WTG}$). The main equation to be solved is,

$$(\boldsymbol{L}, \boldsymbol{D}) = \frac{1}{2}\rho U_{rel}^2 cB(C_L \boldsymbol{e}_L, C_D \boldsymbol{e}_D)$$

where U_{rel} is determined geometrically using information in Figure 2-2. C_L and C_D are taken from tabulated data and determined using the angle of attack (also determined geometrically). In the Navier-Stokes equations, body forces (in unit N/m³) are needed which is why $\boldsymbol{L}$ and $\boldsymbol{D}$ (in unit N/m) are transformed into $\boldsymbol{f}'_{WTG}$ using a local polar grid assuming a thickness of dz (typically in the order of $0.1R$).

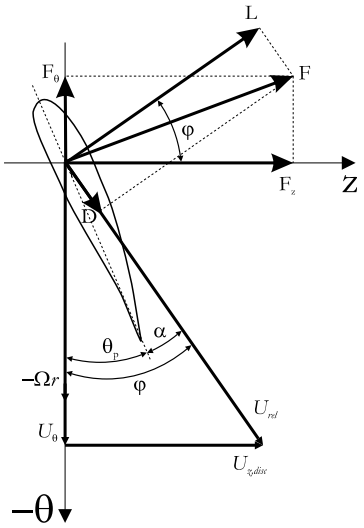

Figure 2-2: Forces and velocities acting on a blade.

The main advantage of the ACD method is that the flow past the rotor is solved without resolving the boundary layer on the blades which significantly reduces the computational demands. The main uncertainties of the method are therefore found in its dependence of the quality of the airfoil data.

2.1.2 Atmospheric model

The shear profile used in the simulations is introduced and maintained using body forces ($\boldsymbol{f}'_{PBL}$). This technique is from now on referred to as the prescribed boundary layer (PBL) technique and is described in detail in Troldborg et al. (2014). There are two main advantages of using the PBL technique compared to traditional simulations in which the shear profile is let to develop in a very long domain or by the use of precursor simulations. The first advantage is that it drastically reduces the simulation time since the precursor simulation step in a PBL simulation only needs to be run in the order of 10-20 time steps. The second advantage is that any given wind profile can be simulated. However, the model is restricted to simulating only neutrally stratified atmospheric conditions.

The atmospheric turbulence is pregenerated using the Mann model (Mann 1994, 1998). The turbulence field, which is referred to as the Mann box, computed by this model is homogeneous, Gaussian, anisotropic, and has the same second order statistics as neutrally stratified atmospheric turbulence and is generated assuming a linear wind profile. By adjusting the roughness length, the velocity, at a certain defined height, in the Mann model, different shear profiles are simulated resulting in different levels of turbulence. The turbulence is imposed in the domain using body forces ($\boldsymbol{f}'_{turb}$) in a plane upstream of the wind turbines. The flow solver is then free to convect the turbulence downstream, pass the turbines.

2.1.3 Computational domain and boundary conditions

All grids used in the simulations are Cartesian. In the EllipSys3D code z refer to the streamwise direction, x spanwise direction and y the vertical direction. The grids are typically structured with an equidistant inner region, where all evaluations are performed according to the grey colored areas in Figure 2-3. Typically, a resolution of $0.1R$ is used in this region. To save computational capacity the grids are stretched towards the lateral, top, inlet and outlet boundaries, according to the white areas in Figure 2-3. The boundary conditions imposed on the different faces of the grid are described in Table 2-1.

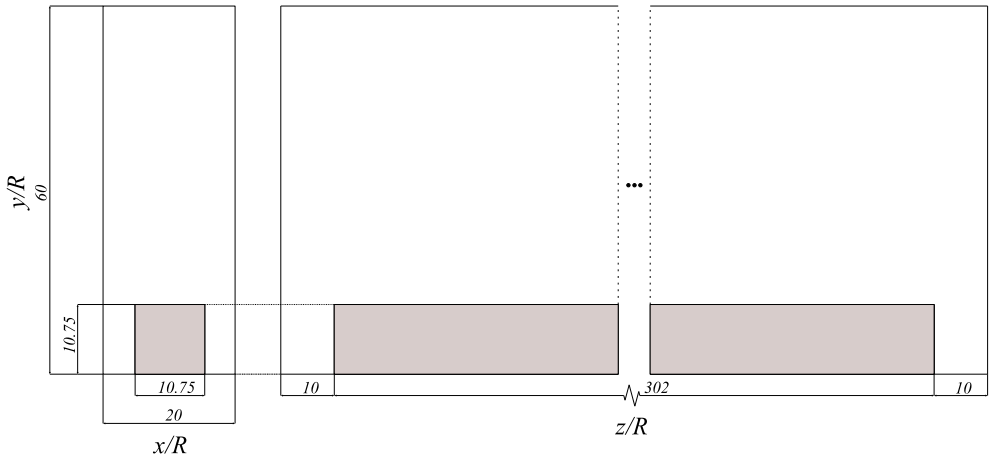

Figure 2-3: A typical grid used in EllipSys3D.

Table 2-1. Boundary conditions

Face	Boundary condition
Inlet	Dirichlet
Outlet	Convective
Bottom	No-slip
Top	Slip
Lateral	Cyclic

2.2 MESOSCALE MODEL DESCRIPTION

The Weather Research and Forecasting (WRF) model is a mesoscale numerical weather prediction system that is suitable for running high-resolution simulations. It is primarily developed at National Centers for Environmental Prediction (NCEP) and National Center for Atmospheric Research (NCAR) in USA. In WRF there are prognostic variables for the horizontal and vertical wind components, potential temperature, geopotential and surface pressure of dry air as well as several scalars such as cloud water and water vapour (Skamarock et al., 2008). To limit the influence from the model boundaries on the result, the modelled domain is significantly larger than the area of interest. A large model domain is also important since the influence from e.g. mountains, oceans or large lakes can have a big impact on the atmosphere in the area of interest even though they are situated far away. To limit the number of grid points in the numerical calculations a nesting

technique is used. Several domains of increasing grid resolution and decreasing geographic coverage are nested inside each other and the numerical equations are solved for each grid point in each domain. This makes it possible to get a very high-resolution result covering only the area of interest.

2.2.1 Wind farm parameterization

The turbines are parameterized as momentum sinks. In every grid box that intersects the rotor disk the horizontal wind component is reduced to represent the drag of the wind turbine (Fitch et al., 2012). Individual turbine specifications can be given for each turbine position.

3 Microscale model development and evaluation

3.1 AIRFOIL DATA SENSITIVITY

As discussed in the previous section, the accuracy of the results when using the ACD method depends on the quality of the tabulated airfoil data. In this study, described in more detail in Nilsson et al. (2014) and Nilsson (2015), the aim is to quantify the uncertainties when using this method. For this purpose, data sets from three different airfoils are used, which are all intended to be representations of the Siemens SWT-93-2.3MW turbine. The first turbine is a downscaled NREL turbine (Jonkman et al. 2009) referred to as AF1. The second turbine is based on the DU21 profile which is one of the profiles used in the AF1 turbine. This profile is used for the entire span width of the rotor. The chord, c, and twist, Φ, distributions are designed to fit the C_P and C_T curves of AF1. This turbine is referred to as AF2. The third turbine, referred to as AF3, is the generic SWT-2.3-93 turbine which is described in detail in Churchfield (2013). The chord and twist distributions of these turbines are shown in Figure 3-1 and Figure 3-2. It is evident that the geometries vary for the different turbines.

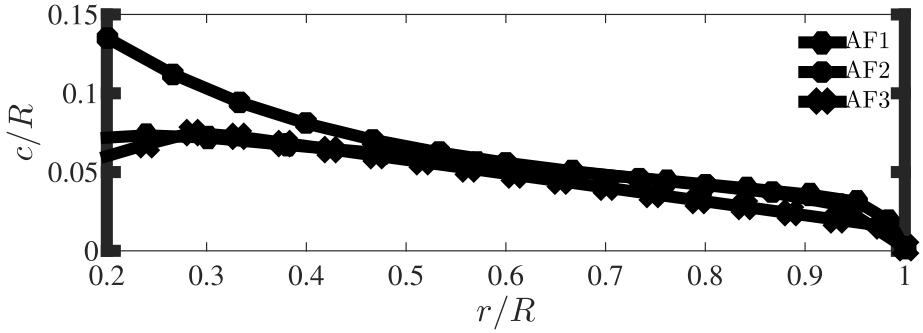

Figure 3-1: Chord distributions.

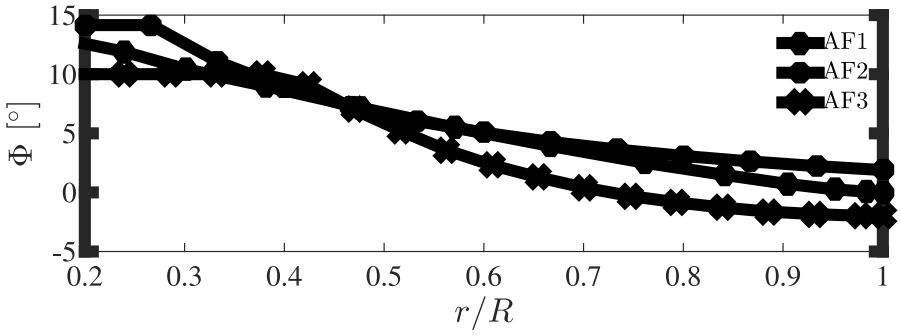

Figure 3-2: Twist distributions.

A row of 8 turbines with a spacing of *6.6R* are simulated in conditions similar to those typical at the Lillgrund wind farm (U_0*=8 m/s, TI=5%)* with the different turbines. The simulation results are compared with real production data extracted at the Lillgrund farm and in Figure 3-3 and Figure 3-4 it can be seen that there is no

large difference between the simulation results when comparing mean relative thrust and power. The agreement with the real production data is also good. The conclusion from this study is that if mean integrated quantities (such as power and thrust) are analyzed, the actual airfoil data has less of importance on the results as long as the turbine size (radius and nominal power) is the same.

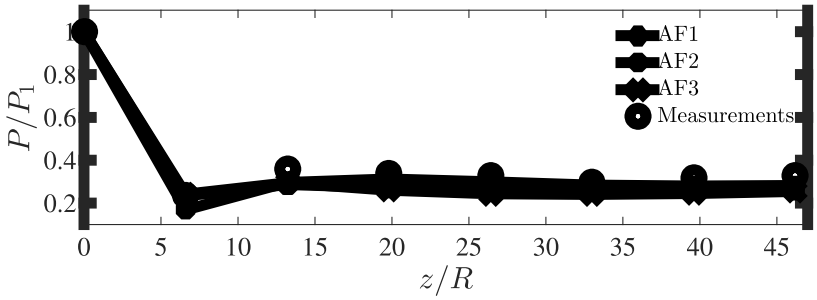

Figure 3-3: Mean relative power.

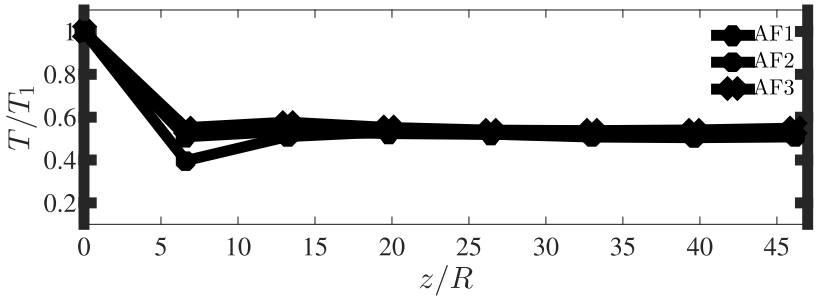

Figure 3-4: Mean relative thrust.

3.2 POWER CONTROL STRATEGY

In order to simulate realistic conditions of variable speed turbines, a power controller needs to be used in order to ensure that the turbines are operating at desired conditions. Below rated power, modern turbines are designed to operate with a constant tip speed ratio, $\lambda = \Omega R/U_0$, regardless of the incoming wind velocity ensuring that the turbine is operating optimally. Here, Ω is the angular velocity and R is the radius of the turbine rotor. The purpose of this study, described in more detail in Nilsson et al. (2015c) and Nilsson (2015), is to quantify the effects of including a power control strategy.

The power control strategy employed in the simulations is based on the following equation,

$$M_{aero} - M_{gen} = I_D \dot{\Omega}$$

Where M_{aero} (aerodynamic torque) and $\dot{\Omega}$ (angular acceleration) are computed by the ACD method. M_{gen} (generator torque) and I_D (moment of inertia of the entire drive train) are inputs and depend on the turbine model used. For further details see Nilsson (2015).

Again, a row of 8 turbines with a spacing of $6.6R$ are simulated in conditions similar to those typical at the Lillgrund wind farm with different control setups

(*IM*: Controlled with moderate I_D, *IL*: Controlled with low I_D, *IH*: Controlled with high I_D, *NC*: Non-controlled (exactly the same case called AF1 in the previous section), *SC*: Rotational speed optimized in a pre-simulation, no active controller). Figure 3-5 shows the comparison of the mean relative power where no large difference are identified. However, when analyzing the mean thrust in Figure 3-6 large difference are found in the NC case compared to the others. This behavior is expected due to the depency of C_P and C_T, respectively, on the tip speed ratio. The conclusion from this study is that a power control strategy is very important if both thrust and loads are evaluated. If only power production is evaluated the power controller is of less importance but it is important to note that the near wake flow, which is largely influenced by the rotor thrust, will be compromised if doing so.

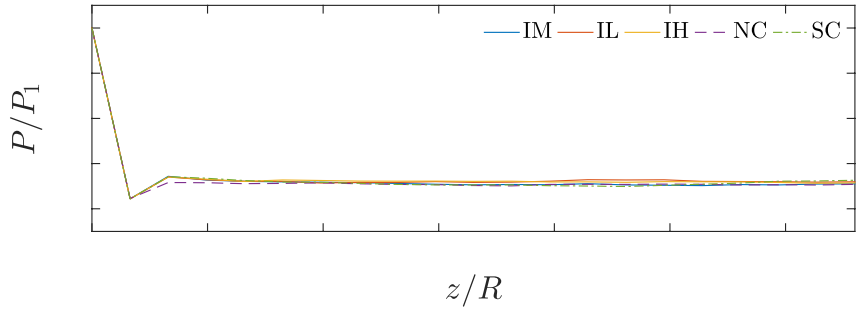

Figure 3-5: Mean relative power.

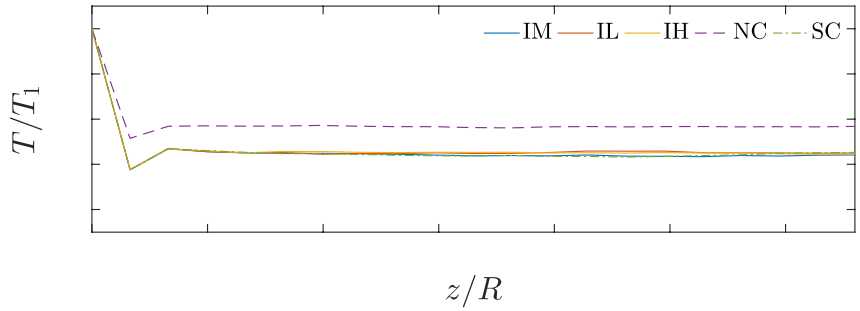

Figure 3-6: Mean relative thrust.

3.3 TURBULENCE EVOLUTION

The procedure of imposing the atmospheric conditions in the simulations is simplified in order to reduce the computational costs. As the turbulence is only forced at the plane location and then being convected downstream by the flow solver, the Mann turbulence will unavoidably evolve and adapt to the flow conditions further downstream. The purpose with this study, which is described in more detail in Breton et al. (2014) and Nilsson (2015), is to evaluate how the turbulence evolve and adapt to the wind profile in a very long domain. In a first step, we use a uniform wind profile with a mean velocity of *8m/s*. We introduce two different Mann turbulence boxes with different intensities. In Figure 3-7, the *TI* (defined as σ_z/U_0) is plotted as function of the downstream distance.

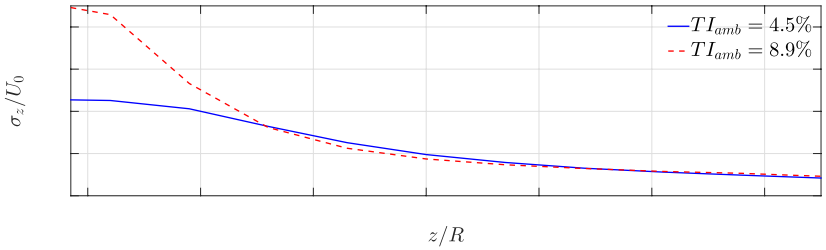

Figure 3-7: Turbulence intensity as function of downstream distance.

It is clear that the *TI* level at first is different in the two runs, and that that curves approaches the same value as progressing downstream. In this case, since we do not have a shear profile to sustain the turbulence production, the curves would eventually approach *zero* if the domain was long enough. In a second step, we use a shear profile and introduce the two Mann turbulence boxes mentioned above. In Figure 3-8, we see that the *TI* level is different initially and that curves approaches the same value further downstream. In this case we have a shear profile to sustain the turbulence production which is why the value approaches approximately *0.045* instead of *zero*.

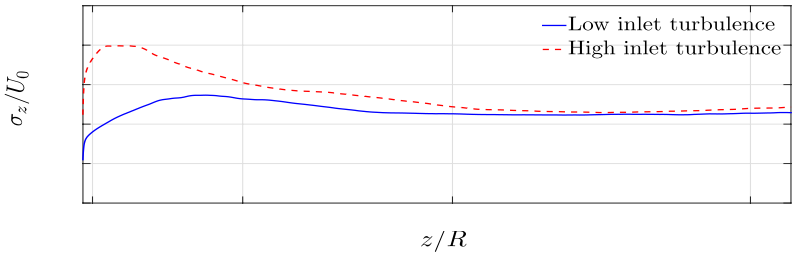

Figure 3-8: Turbulence intensity as function of the downstream distance.

From a power production perspective, which depends partly on the ambient *TI* level, this implies that depending on at which downstream position you place your wind turbines and how long your farm is, the estimated production will differ. To assess this, 10 aligned turbines are placed at different downstream positions in relation to the Mann box plane (L_{MANN}) according to Figure 3-9 (where $L_{T1,WTG1}=17R$, $L_{T3,WTG1}=168R$). The inflow is from the left. In Figure 3-10 the mean relative production results are depicted (red curves use the high inlet turbulence, blue curves the low inlet turbulence).

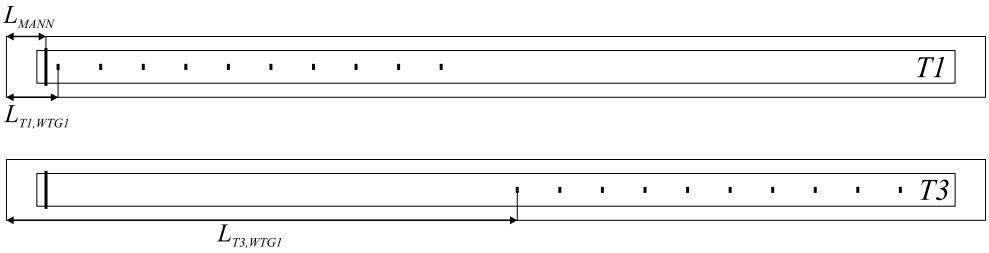

Figure 3-9: Positions of turbines in the domain.

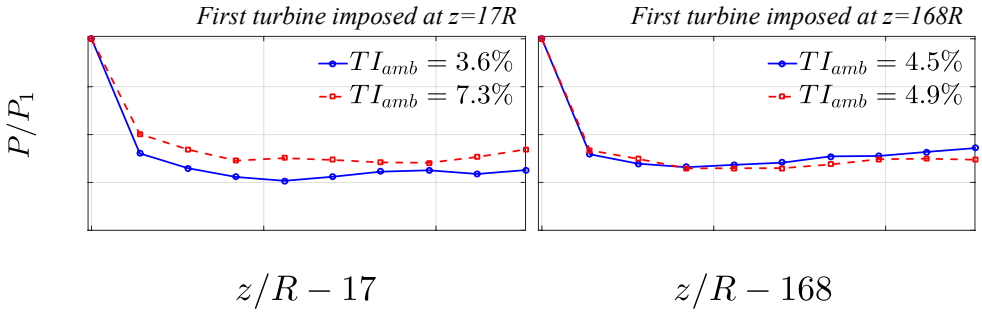

Figure 3-10: Mean relative power.

3.4 NUMERICAL AND PHYSICAL PARAMETERS IN LONG DOMAINS

Micro scale simulations are typically used for simulation of single turbines or flows inside a wind farm. When modelling very long wakes, such as farm wakes, the result is subject to increased uncertainties.

3.4.1 Sensitivity to numerical and physical parameters

The first parameter study (Eriksson et al., 2014) is performed for a row of 10 turbines, see Figure 3-11 and Figure 3-12, with focus on the sensitivity of the simulation results to the numerical parameter grid resolution (*dz*) and the physical parameter turbulence intensity (*TI*).

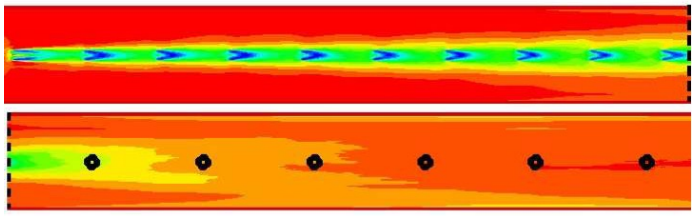

Figure 3-11: The streamwise wind speed at hub height for a row of turbines with the internal spacing 14 R. The up-per portion covers the first part of the domain and con- tinues (behind the row) in the lower portion showing the farm wake in which each km (21.5 R) is marked with circcles.

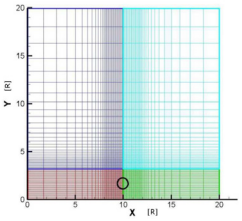

Figure 3-12: The equidistant region of the grid is 4R*4R. The disc is shown by the circle.

The level of the ambient turbulence has a large impact on both the relative production and the wake recovery, see Figure 3-13. A higher ambient turbulence level gives an increased mixing and a higher recovery of velocity inside and behind the farm. It can also be seen that higher ambient turbulence levels results in higher relative production values.

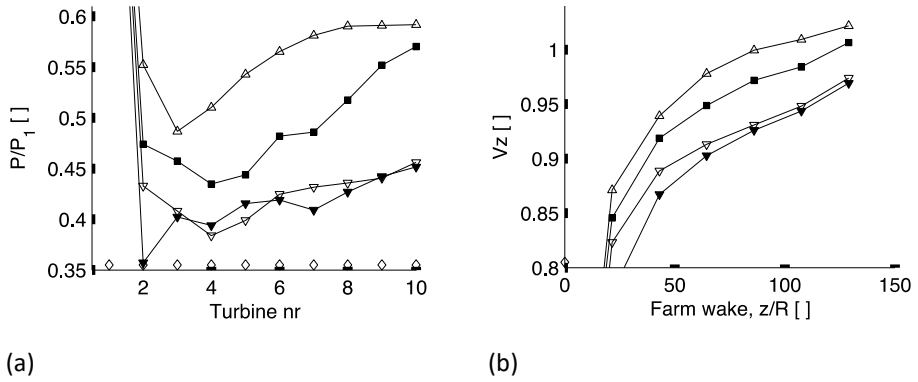

Figure 3-13: The impact of turbulence intensity for a) Relative production, turbine 2-10. b) Velocity recovery.
Legend: ——△——TI=11%,—— ■ ——TI=6.3%,——▽——TI=3%, ——▾—— TI = 0 %, ♦Turbine position (z)

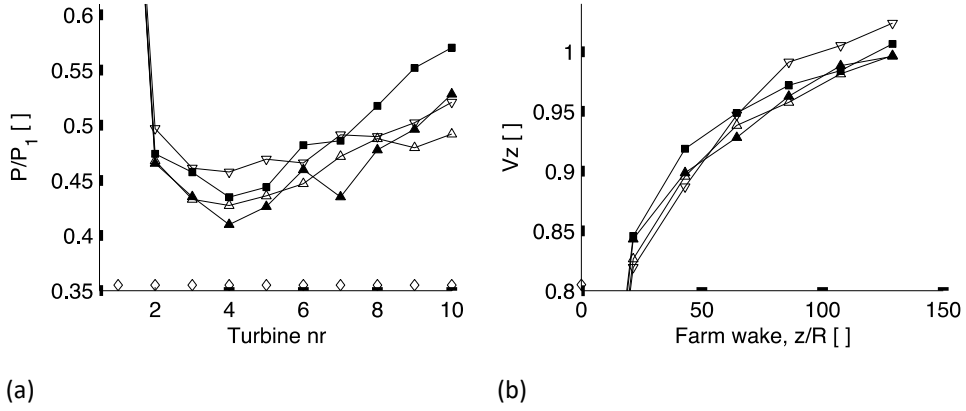

Figure 3-14: Dependency of grid resolution for a) Relative production, turbine 2-10. b) Velocity recovery.
Legend: ——▲——dz=0.05R,——△——dz=0.067R,—— ■——dz=0.1 R, ——▽—— dz =0.13 R, Turbine position (z) ◆

The impact on the relative production and the wake recovery of using different grid resolutions is depicted in Figure 3-14. Here it is hard to see any clear trends. The conclusion from this study is that the grid has a limited impact when compared to the ambient turbulence level. Similar results were discovered in Nilsson et al. (2015), leading to the usage of a grid resolution of *0.1R* which is found to be a good compromise between required computational capacity and numerical accuracy.

3.4.2 Sensitivity to extensions of domain and turbulence box

In a second parameter study (Eriksson et al., 2015a) the focus is on the sensitivity to the extensions of the domain, equidistant region and turbulence box, see Figure 3-15, as these parameters potentially (due to blockage, smearing and turbulence mixing) could impact the downstream trends.

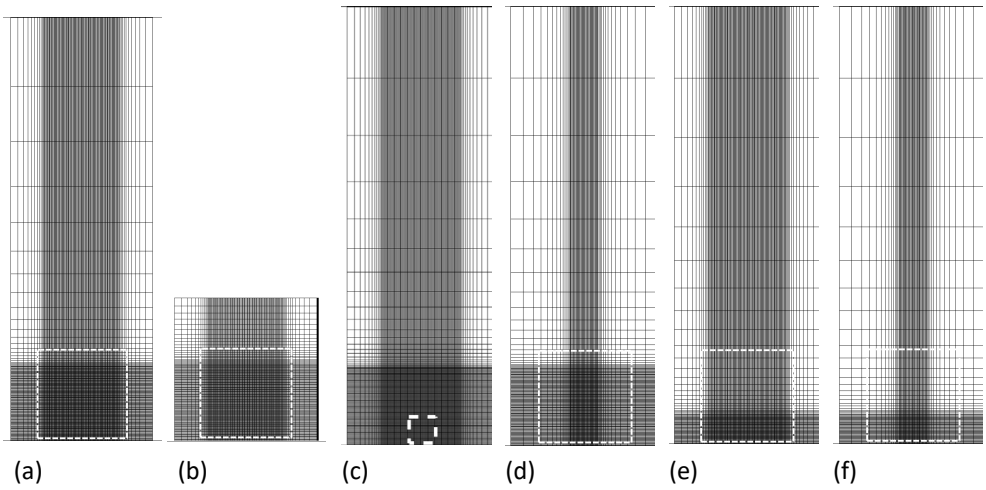

Figure 3-15 The grid (in the x-y plane) and extension of the turbulence box (marked with dashed white lines) for (a) Reference case (Ref), (b) Lower domain (Low), (c) Turbulence box -small (Turb s), (d) Equidistant region: High/narrow: (Eqv h), (e) Equidistant region: Wide/low (Eqv w), (f) Equidistant region: Small (Eqv s).

In Figure 3-16a, it could be seen that there were some blockage effects present in the first parameter study (comparable to case (Low)) which explains the downstream increase of relative power. Also, the turbulence box needs larger extensions to allow mixing from surrounding flow to a larger extent, see Figure 3-16b. Another part of the explanation can also be found if a small equidistant region is used that smears out the outside part of the wake. For the long-distance wake, see Figure 3-17, the size of the turbulence box has the largest impact.

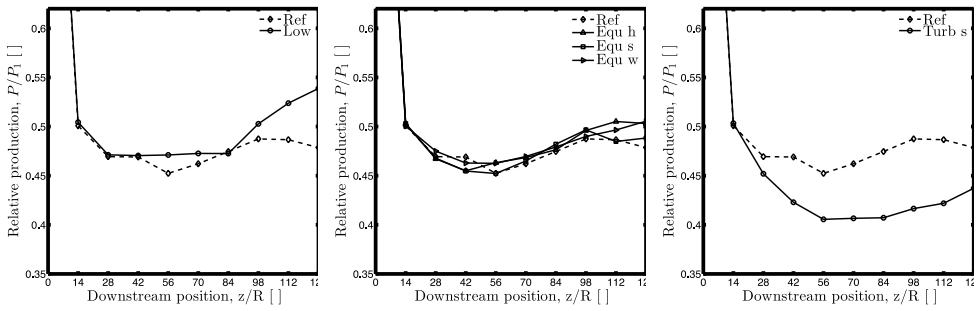

Figure 3-16: Impact on relative production. Due to a) height of domain b) size of equidistant region c) size of turbulence box.

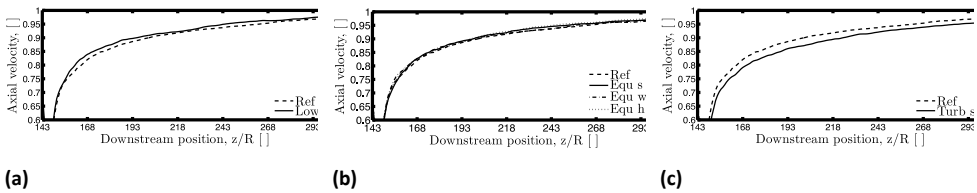

Figure 3-17: Impact on velocity at hub height in the long distance wake behind the wind farm. Due to a) height of domain b) size of equidistant region c) size of turbulence box

4 Initial analysis of Wind turbine loads in Lillgrund

In 2010 Siemens and Vattenfall decided to start evaluating structural loads in Lillgrund, and for this purpose six selected turbines in the south-west corner (Figure 4-1) were equipped with additional sensors in e.g. tower and blades. The main idea was to study interactions between turbines in the straight row pattern, and different pre-set curtailment campaigns where designed. Vattenfall and Teknikgruppen have later selected a 9-month period from March to November for a detailed assessment. During this period the curtailment pre-set pattern was not changed, and the overall data quality was found to be sufficient.

Turbine position ID
B6
B7
B8
C8
D7
D8

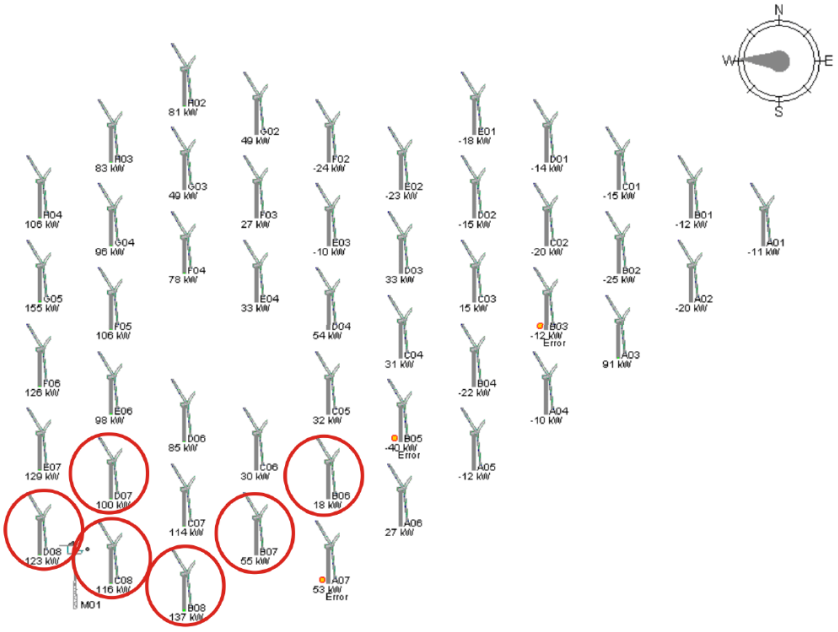

Figure 4-1 Turbines in the south-west corner selected for the load measurements [B6 , B7 , B8 , C8 , D7 , D8].

For the selected campaign, 5 additional turbines where added to the experiment, together with a set-up for running turbines with different pitch-rpm schedules, in order to facilitate changes of the thrust characteristics for upwind turbines. Thus, turbines A5, A6, A7, C7 and E7 were included only to add more possibilities to modify turbine interactions. A scheme for running the south-west corner of Lillgrund with four different curtailment settings is presented in Table 4-1. Here

the occurrence of steady mean wind directions ±15° from the fundamental directions 120° and 222° triggered sequences of 30 min periods where two different thrust upstream settings were altered. In addition, the 180° diagonal was included to increase the number of turbine pairs for the assessment.

Table 4-1. Organization of the curtailment schedule.

	120+/-15°		180+/-15°		222+/-15°	
	1st 30 min.	2nd 30 min.	1st 30 min.	2nd 30 min.	1st 30 min.	2nd 30 min.
A05	A	B	A	B		
A06	C	A	C	A	D	D
A07	A	B	A	B	A	D
B07					A	B
B08			D	D	D	D
C07			A	B		
D07					A	C
D08			D	D	D	D
E07			A	C		

Convenient analysis of this kind of complex experiment require that the different data sets are merged together through the processing of statistics with a common time axis. The data sources to align where here A) a curtailment log with the actual curtailment setting for each of the 9 curtailed turbines, B) the Lillgrund 0.1 Hz raw SCADA signals for 48 turbines containing the basic turbine data such as active power, nacelle wind speed, nacelle wind direction, nacelle direction etc. C) 10 Hz load and vibration signals for 6 turbines according to Figure 4-1. Monthly tables of statistics were then produced for 10 min, 5 min and 2.5 min averaging time. An overview of the content is presented (block-wise) in Table 4-2. Examples of plotting the monthly statistics are shown in Figure 4-2.

Table 4-2. Layout of blocks in the compiled monthly statistics files.

Block	Description
A)	Time block SCADA (5 columns, starting from column 1) Year Month Day Hour Minute
B)	Time Block Siemens (5 columns, starting from column 6) Year Month Day Hour Minute
C)	Curtailment Block-Siemens (18 columns, starting from column 11) 1-9: curtailment mode:(0 =>- or OFF,1 => A,2 => B,3 => C,4 => D) 10-18: curtailment sequence: i.e. 2 => second *T* min sequence within curtailment mode, 3 => third etc. (Turbine Order [A05,A06,A07,B07,B08,C07,D07,D08,E07])
D)	Data Block SCADA (1536 columns, starting from column 29) 48 turbines / 32 quantities per turbine => 1536 columns 8 signals: [WindSp NacDir ActPow Rpm p1 p2 p3 pref] x 4 quantities per signal (order: mean min max std) = 32
E)	Data Block Siemens (342 columns, starting from column 1564) 6 turbines / 57quantities per turbine => 342 columns Turbine order [B07, B08, D08, C08, B06, D07]

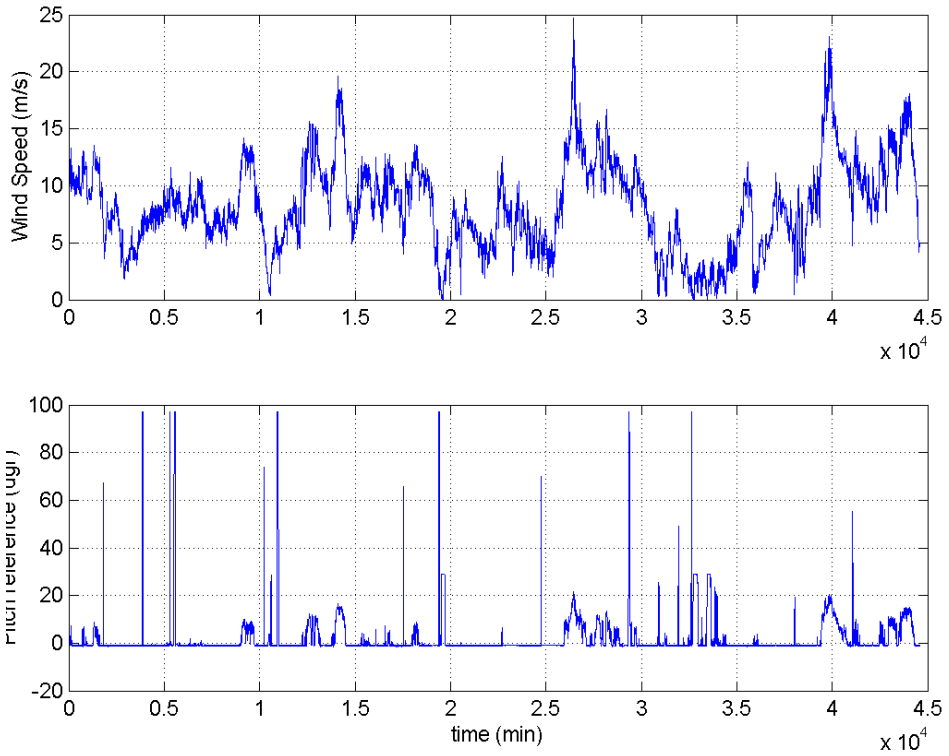

Figure 4-2 Consecutive 10min averages of nacelle wind speed and blade pitch angle for turbine B8 during March 2018.

The high frequency load measurements will over time generate a huge amount of data. One way to find inspiration for data processing is to find situations of interest through plotting the statistics, and then select shorter sequences for more detailed assessment. For this second step, an efficient overview sheet was designed, where

1 hour of high frequency load and vibration signals are plotted on the same page. The plot sheets where then stored for convenient access as individual pdf files, in a month/day/turbine/hour structure. In addition to the load and vibration signals, a plot of the curtailment history (all 9 turbines) was included. An example of a plot sheet for turbine C8 is presented in Figure 4-4.

Load quantities in the statistics file are processed as [mean,min,max,std], but also as Damage Equivalent Loads. Two examples of how the statistics files can be used to evaluate the effects of the different curtailment settings, are presented if figure xx and xxx, where the interaction between turbines A6 and B6 in the 120±15° sector is analyzed for wind speed bins 7-8, 8-9, 9-10 and 10-11 m/s. Figure 4-4 shows intensity of generator torque intensity (std/mean) comparing curtailment settings C and A. In Figure 4-6 the same sector, wind bins and curtailments are chosen, but here the load related quantity is the standard deviation of longitudinal nacelle vibration. It is here evident that curtailment C for the 7-8 m/s bin result in a significant reduction of loads in generator and tower compared to curtailment A, but for the higher winds the difference is much less pronounced.

The data processing activities outlined above is intended to save valuable time when this combined data set is used for future R&D objectives. The number of high resolution signals available, combined with the interesting Lillgrund wind farm layout, will open up for a wide variety of interesting investigations.

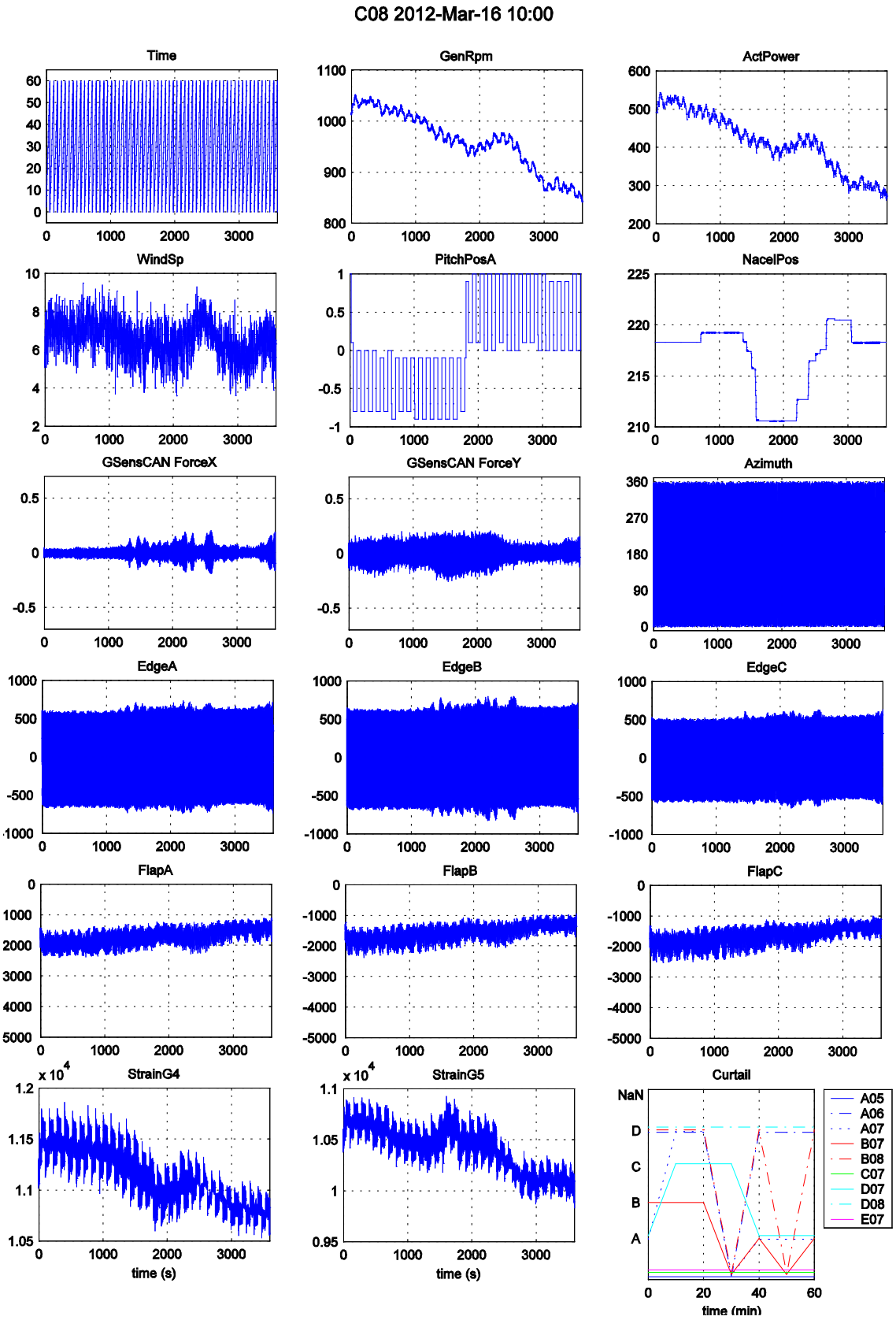

Figure 4-3 1 hour overview plots for turbine C8. In the lower right corner the curtailment history is shown.

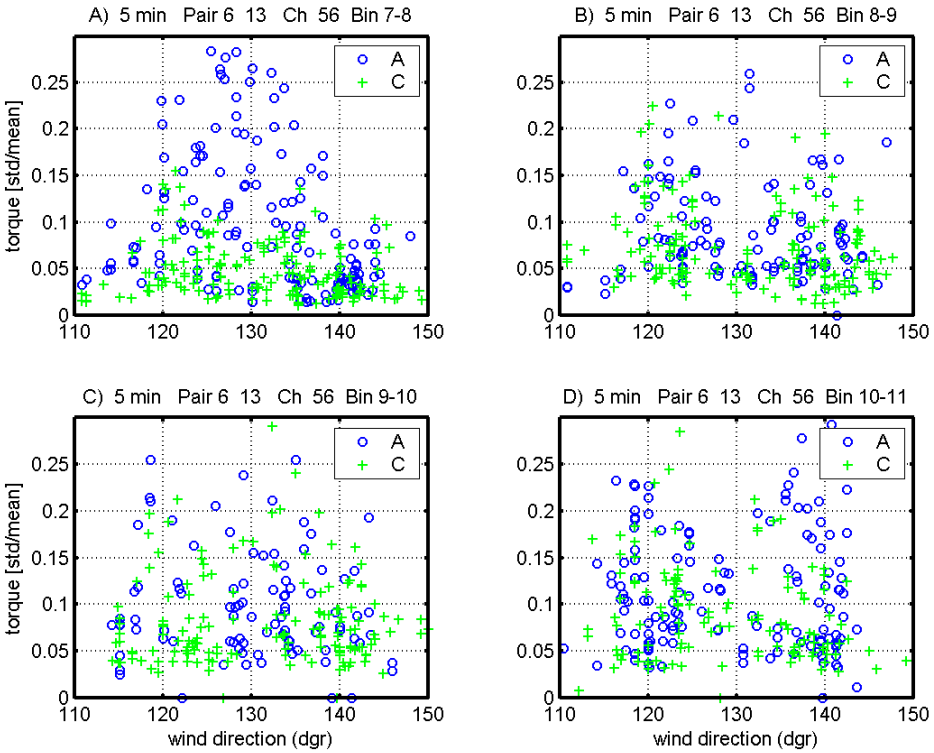

Figure 4-4 Intensity of generator torque variation (std/mean) in turbine B6 (13) when upstream turbine A6 (6) is run with curtailment settings A and C respectively (wind speed bins 7-8, 8-9, 9-10 and 10-11 m/s).

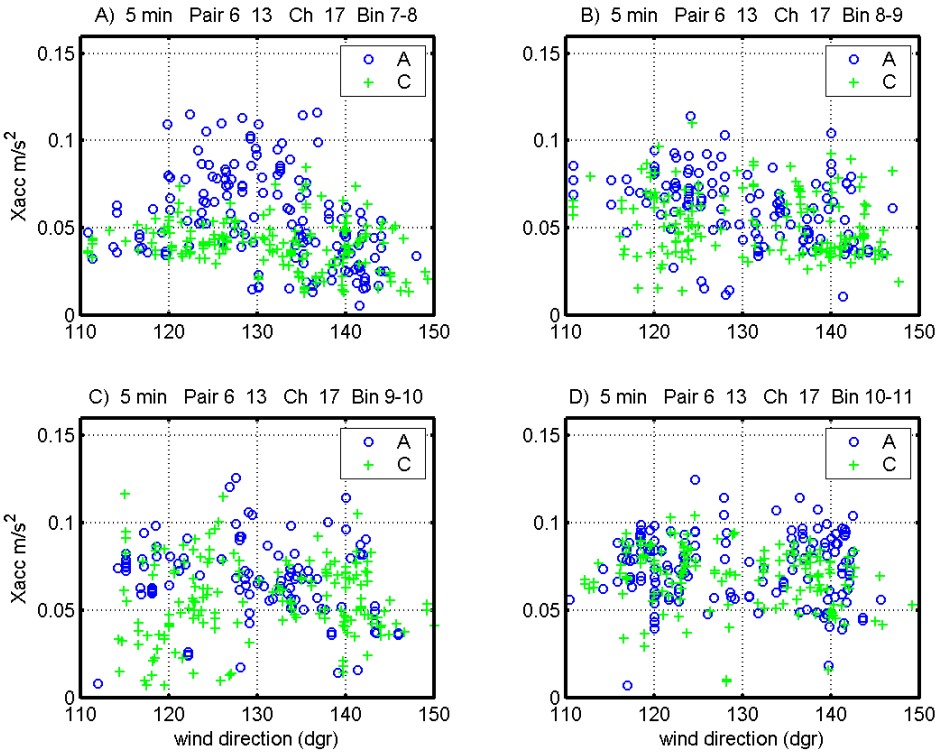

Figure 4-5 Standard deviation of longitudinal nacelle acceleration in turbine B6 (13) when upstream turbine A6 (6) is run with curtailment settings A and C respectively (wind speed bins 7-8, 8-9, 9-10 and 10-11 m/s).

5 Farm simulation results

5.1 LILLGRUND WIND FARM (MICROSCALE)

The Lillgrund wind farm is situated offshore between Sweden and Denmark and consists of 48 wind turbines, as depicted in Figure 5-1. Compared to other offshore wind farms, the turbines in the Lillgrund farm are positioned very tightly, with internal turbine spacings as small as 6.6R, where R = 46.5m is the rotor radius. The farm efficiency of Lillgrund is therefore lower in comparison to other wind farms but thanks to the characteristics of the farm it is very interesting from a wake interaction point of view. Therefore, it is used for validating the LES/ACD approach by comparing measured with simulated power production. This section presents the main results from Nilsson et al. 2015b.

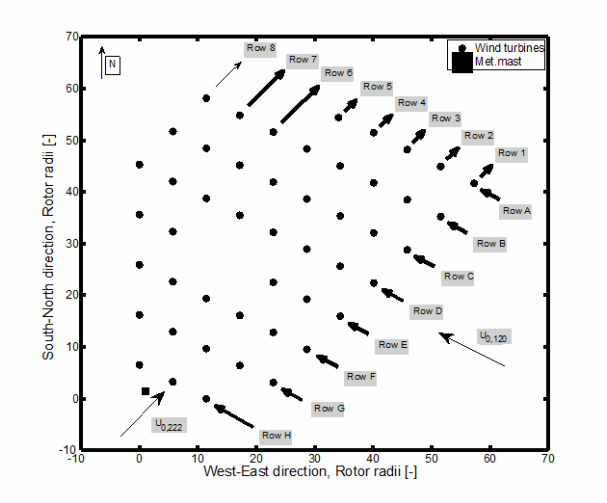

Figure 5-1: Layout of the Lillgrund wind farm.

The simulations are performed using flow conditions determined from measurements. The atmospheric turbulence is modeled using synthetic turbulence created by the Mann model (Mann 1994, 1998) characterized by a turbulence intensity of 5.7%. The PBL is defined by the power law with a shear exponent equal to *0.11*. Two inflow angles (*120±2.5°* and *222±2.5°*) are considered in the analysis, as denoted by the black arrows in Figure 3.1, but only the *120±2.5°* case is presented here for the sake of conciseness. The power production is filtered for $7.5 \leq U_0 \leq 8.5 m/s$ and is normalized with the median production of Row 1 in Figure 5-1. In Figure 5-2, the average production of all full-length rows (Rows B-D) is depicted. The general agreement between the simulations and the measurements is very good. However, there are small discrepancies in the agreement, where an overestimation of the power for the second turbine in the row is observed in the simulation results.

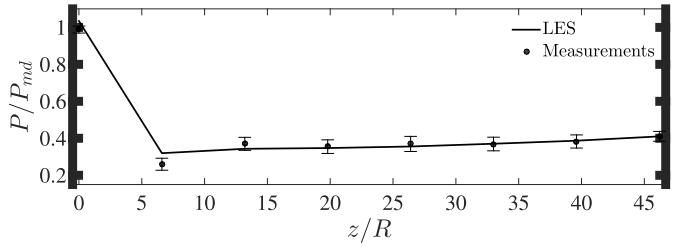

Figure 5-2: Mean relative production.

In Figure 5-3 the production of Row E turbines is shown. This row is of special interest since it contains of a hole in the middle where no turbines are placed and where the flow is allowed to recover over a longer distance. The production is again slightly overestimated for the second turbine in the row and also for the turbines after the recovery hole. The production of the turbines after the hole is observed to have a similar trend compared to the measurements. It is worth noting that the production after the recovery hole is almost twice as high as the production before the hole, which shows the effects of placing the turbines so close to each other.

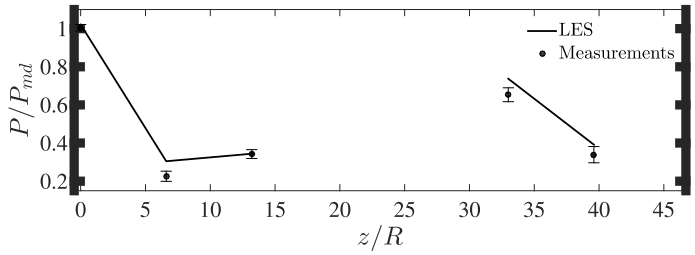

Figure 5-3: Mean relative production.

A simple power curtailment study is performed to determine how the total production of the farm changes when the power extraction of the front row turbines is decreased. The power curtailment is performed by pitching the blades 2°, 4°, and 6° which allows more kinetic energy to pass to the downstream turbines which will, ideally, experience increased production and decreased loads. In Figure 5-4, which is based on the average production of all full-length rows (Row B-D) normalized with the median production of Row 1 for the 0° pitch case, it can be seen that only the second turbine in the row benefits from the curtailment and that the increase in production at this turbine is lower than the loss at the first turbine. This simple curtailment strategy does not, in other words, increase the overall production of the farm and more advanced strategies needs to be evaluated.

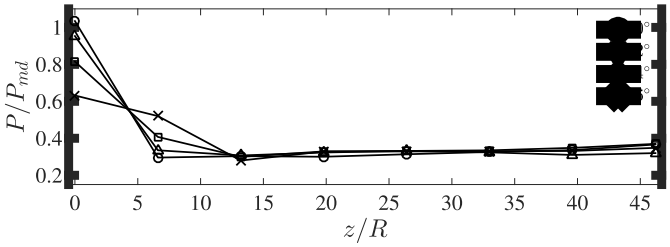

Figure 5-4: Mean relative production.

5.2 FARM BLOCKAGE (MESOSCALE)

The interaction between a wind farm and the atmosphere causes a decrease in wind speed upstream of the wind farm. This study aims to, by means of atmospheric modelling, investigate this blockage effect and its sensitivity to the size and layout of the wind farm.

In this study, an idealized model setup was used in order to investigate blockage effects. Radiation, surface and microphysics parameterization options where turned off and the Coriolis factor was set to 0 in the model setup.

A two-domain setup with one-way nesting was used. The parent domain had a horizontal resolution of 333m and periodic boundary conditions while the child domain had a resolution of 111m.

Two wind farms were studied. For each wind farm the model was run with 2 different wind farm configurations, one with the full wind farm layout and one with only the front row relative to the wind direction. The model was also run for 2 different stability cases, neutral and slightly stable. The vertical profiles of potential temperature for the two stability cases are shown in Figure 5-5.

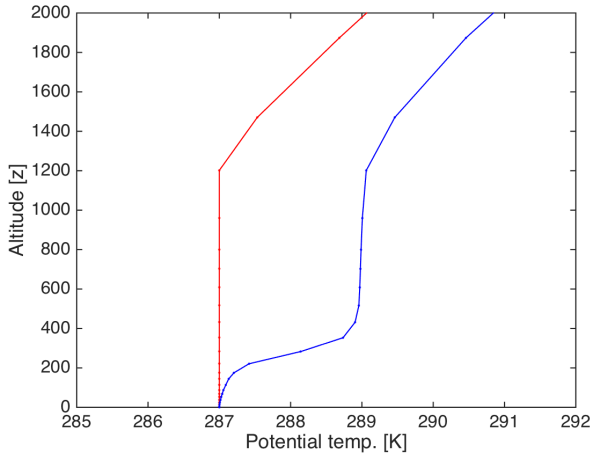

Figure 5-5. Profiles of potential temperature used to initialize the model. Neutral case in red and Stable case in blue.

5.2.1 Wind farm 1

A schematic of the two different wind farm configurations used is shown in . Power and thrust curves from a 7MW turbine with 154m rotor diameter and 97m hub height was used. The idealized model runs were set up to achieve a westerly free stream wind speed of approximately 9m/s at hub height (97m). Two stability classes and two configurations resulted in a total of four cases (Table 5-1).

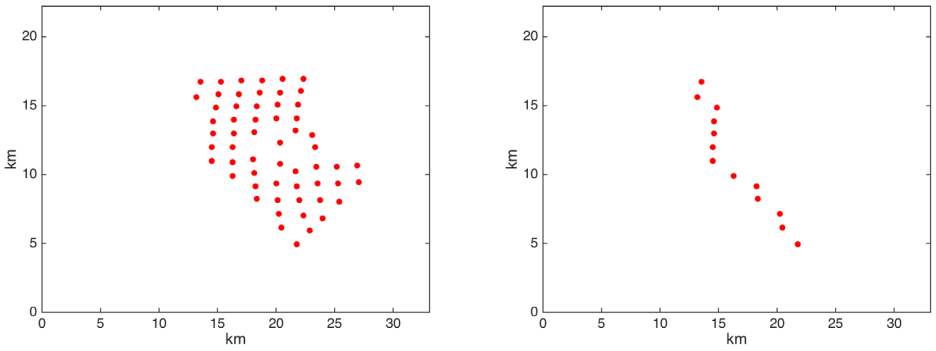

Figure 5-6. Model domain with 111m horizontal resolution and wind turbine configuration Full (left) and Only 1 row (right).

Table 5-1. Model configuration cases.

Case	Wind turbine configuration	Stratification
1	Full	Neutral
2	Only 1 row	Neutral
3	Full	Stable
4	Only 1 row	Stable

Average power and wind speed at hub height for the front row relative to the wind direction for the two layouts are given in Table 5-2.

Table 5-2. Model configuration cases.

	Neutral			Stable		
	Full	1 row	Diff (%)	Full	1 row	Diff (%)
Avg. Power (kW)	2512	2520	0.3	3146	3175	0.9
Avg. Wind Speed (m/s)	7.94	7.94	0.1	8.54	8.57	0.3

In Figure 5-7 the normalized wind speed as a function of distance from the front row turbine is shown for the neutral and stable cases.

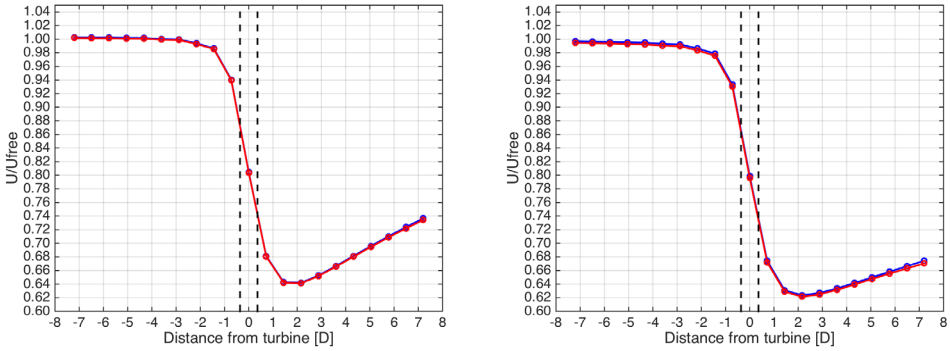

Figure 5-7. Neutral (left) and stable (right) case wind speed normalized by free stream wind speed as a function of distance from wind turbine position in rotor diameters. Results for full layout in red and front row layout in blue. Horizontal bounds of model grid box representing turbine are marked by dashed black lines.

The differences in the model results between only one row of turbines and a large wind farm are quite small but noticeable and consistent throughout all cases. In the neutral (stable) case the upstream row has ~0.3% (~0.9%) less power when the entire wind farm is present compared to when there is only one row of turbines.

5.2.2 Wind farm 2

A schematic of the two different wind farm configurations used is shown in . Power and thrust curves from 8.4MW turbine with 167m rotor diameter and 103.5m hub height was used. The idealized model runs were setup to achieve a free stream wind speed of approximately 9.5m/s at hub height (103.5m). The direction of the flow in the model domain is along the positive x-axis, which can be translated to from left to right in Figure 5-8.

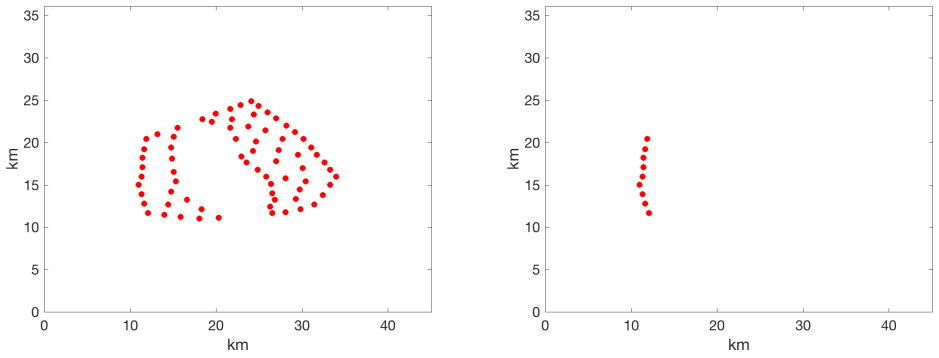

Figure 5-8. Model domain with 111m horizontal resolution and wind turbine configuration Full (left) and Only 1 row (right).

To achieve different wind direction cases the wind farm layout was rotated and the flow direction was held constant. Two stability classes, two configurations and four wind directions resulted in a total of 16 cases (Table 5-3).

Table 5-3. Model configuration cases.

Case	Wind direction	Stratification	Wind turbine configuration
1	W	Neutral	Full
2			Only front row
3		Stable	Full
4			Only front row
5	WNW	Neutral	Full
6			Only front row
7		Stable	Full
8			Only front row
9	NE	Neutral	Full
10			Only front row
11		Stable	Full
12			Only front row
13	WSW	Neutral	Full
14			Only front row
15		Stable	Full
16			Only front row

Wind direction W

The wind farm layout used in W wind directions is illustrated in Figure 5-8.

Average power and wind speed at hub height for the front row relative to the wind direction for the two layouts are given in Table 5-4.

Table 5-4. Model configuration cases.

	Neutral			Stable		
	Full	1 row	Diff (%)	Full	1 row	Diff (%)
Avg. Power (kW)	4343	4383	0.9	4339	4399	1.4
Avg. Wind Speed (m/s)	8.95	8.98	0.3	8.98	9.02	0.5

In Figure 5-9 the normalized wind speed as a function of distance from the front row turbine is shown for the neutral and stable cases.

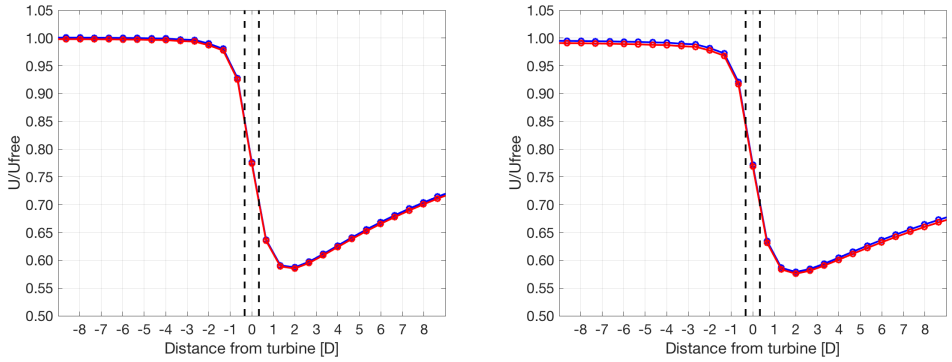

Figure 5-9. Neutral (left) and stable (right) case wind speed normalized by free stream wind speed as a function of distance from wind turbine position in rotor diameters. Results for full layout in red and front row layout in blue. Horizontal bounds of model grid box representing turbine are marked by dashed black lines.

Wind direction WNW

The wind farm layout used in WNW wind directions is illustrated in Figure 5-10.

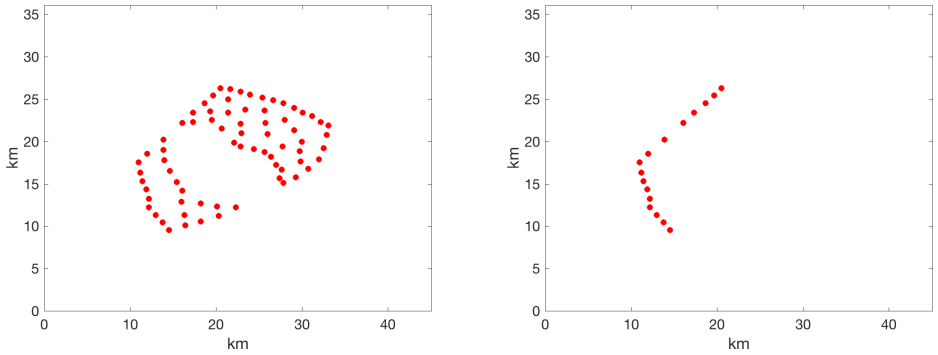

Figure 5-10. Model domain with 111m horizontal resolution and wind turbine configuration Full (left) and Only 1 row (right).

Average power and wind speed at hub height for the front row relative to the wind direction for the two layouts are given in Table 5-5.

Table 5-5. Model configuration cases.

	Neutral			Stable		
	Full	1 row	Diff (%)	Full	1 row	Diff (%)
Avg. Power (kW)	4332	4366	0.8	4337	4401	1.4
Avg. Wind Speed (m/s)	8.94	8.96	0.3	8.97	9.02	0.5

In Figure 5-11the normalized wind speed as a function of distance from the front row turbine is shown for the neutral and stable cases.

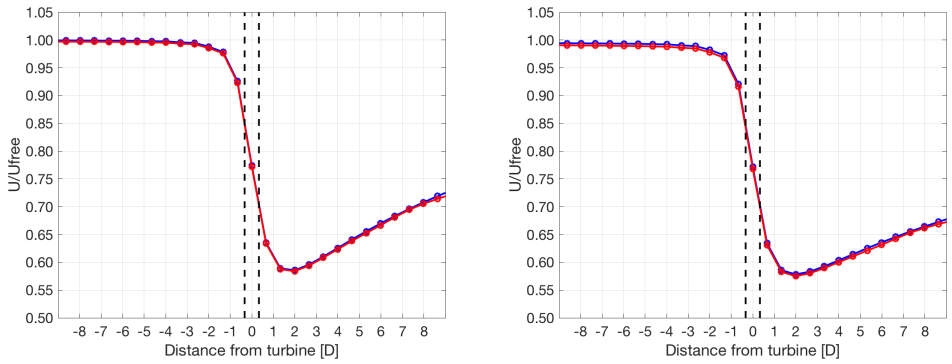

Figure 5-11. Neutral (left) and stable (right) case wind speed normalized by free stream wind speed as a function of distance from wind turbine position in rotor diameters. Results for full layout in red and front row layout in blue. Horizontal bounds of model grid box representing turbine are marked by dashed black lines.

Wind direction NE

The wind farm layout used in NE wind directions is illustrated in Figure 5-12.

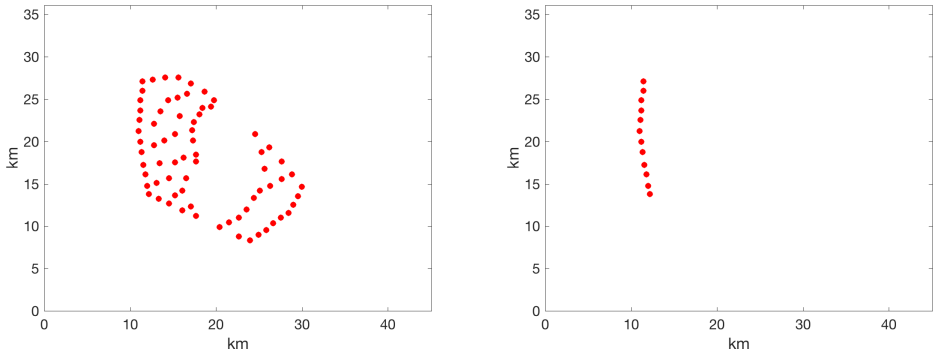

Figure 5-12. Model domain with 111m horizontal resolution and wind turbine configuration Full (left) and Only 1 row (right).

Average power and wind speed at hub height for the front row relative to the wind direction for the two layouts are given in Table 5-6.

Table 5-6. Model configuration cases.

	Neutral			Stable		
	Full	1 row	Diff (%)	Full	1 row	Diff (%)
Avg. Power (kW)	4316	4365	1.1	4311	4389	1.8
Avg. Wind Speed (m/s)	8.94	8.97	0.4	8.96	9.01	0.6

In Figure 5-13 the normalized wind speed as a function of distance from the front row turbine is shown for the neutral and stable cases.

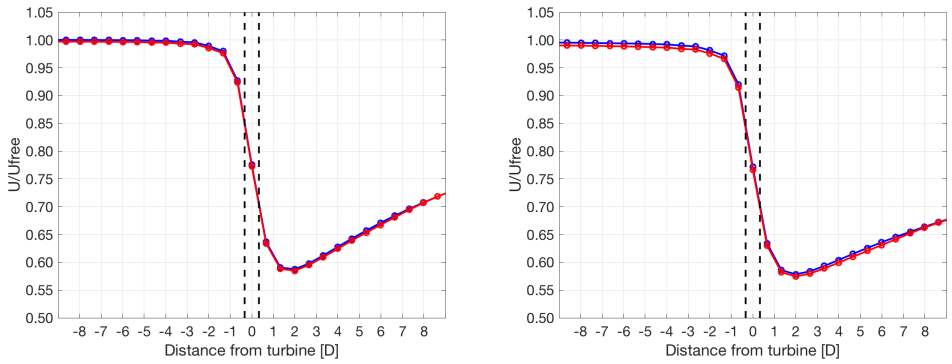

Figure 5-13. Neutral (left) and stable (right) case wind speed normalized by free stream wind speed as a function of distance from wind turbine position in rotor diameters. Results for full layout in red and front row layout in blue. Horizontal bounds of model grid box representing turbine are marked by dashed black lines.

Wind direction WSW

The wind farm layout used in WSW wind directions is illustrated in Figure 5-14.

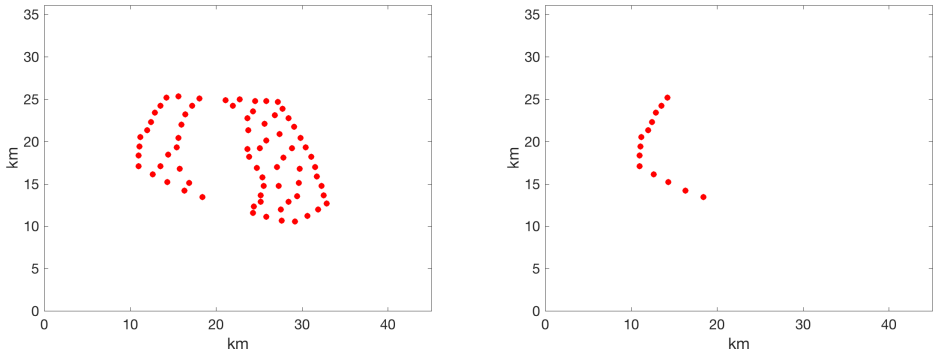

Figure 5-14. Model domain with 111m horizontal resolution and wind turbine configuration Full (left) and Only 1 row (right).

Average power and wind speed at hub height for the front row relative to the wind direction for the two layouts are given in Table 4-7.

Table 5-7. Model configuration cases.

	Neutral			Stable		
	Full	1 row	Diff (%)	Full	1 row	Diff (%)
Avg. Power (kW)	4361	4391	0.7	4354	4402	1.1
Avg. Wind Speed (m/s)	8.96	8.98	0.2	8.89	9.02	0.4

In Figure 5-15 the normalized wind speed as a function of distance from the front row turbine is shown for the neutral and stable cases.

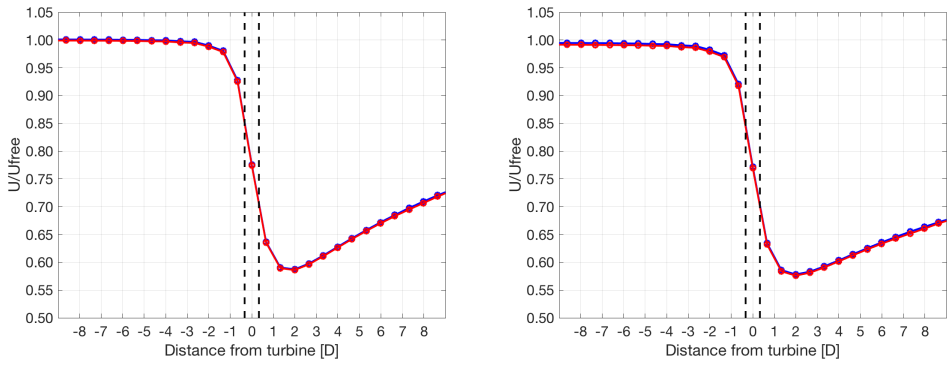

Figure 5-15. Neutral (left) and stable (right) case wind speed normalized by free stream wind speed as a function of distance from wind turbine position in rotor diameters. Results for full layout in red and front row layout in blue. Horizontal bounds of model grid box representing turbine are marked by dashed black lines.

In summery the differences in the model results between only one row of turbines and a large wind farm are quite small but noticeable and consistent throughout all cases. Average percentage differences in power between a full farm layout and only the front row relative to the wind direction for four wind directions are given in Table 5-8.

Table 5-8. Average percentage difference in power between a full farm layout and only front row.

Wind direction	Neutral	Stable
W	0.9	1.4
WNW	0.8	1.4
NE	1.1	1.8
WSW	0.7	1.1

6 Farm-farm simulation results

The most suitable sites for offshore wind farms are limited by, for example, a certain range of water depth and distance from shore. In for example countries with high goals for wind energy integration and short coastlines wind farms will need to be built in relatively close proximity to other wind farms.

As more offshore wind farms are built there will be more occasions when the wake from one wind farm will interact with other nearby wind farms, in so called wind farm clusters. Looking at the planned projects it becomes apparent that many projects will be quite near to each other (Eriksson et al., 2012a).

This development makes it interesting to not only study the near and far wakes behind single turbines and the interaction inside farms but also the long-distance wakes impacting the wind conditions at neighboring sites. With the coming development better knowledge is needed to ensure better production and load estimations, especially when other wind farms are close and will interact with each other. This interaction between farms is called farm to farm interaction.

A range of studies on wakes behind wind turbines and their interactions inside wind farms are available, but there are far fewer published studies looking at the long-distance wakes which occur behind entire wind farms. The distances that are looked at for long distance wakes are significantly greater than those of near wakes, where the properties of the rotor can clearly be seen, and far wakes, where the interaction between wind turbines is in focus. A further description of earlier studies of wakes is presented in Eriksson (2015).

6.1 LONG DISTANCE WAKES (MICROSCALE)

6.1.1 Lillgrund wind farm

The full wind farm of Lillgrund is simulated, including the long distance wake up to 7 km downstream from the last turbine, in Eriksson et al. (2015b).

The grid, the equidistant region and the turbulence plane were chosen with relatively large extensions. To avoid the region of distortion the first turbine was placed 75 R behind the Mann plane. The layout of the wind farm is seen in Figure 6-1, the studied flow direction is along the z-axis. The result is illustrated in Figure 6-2 for the velocity and in Figure 6-3 for the turbulence.

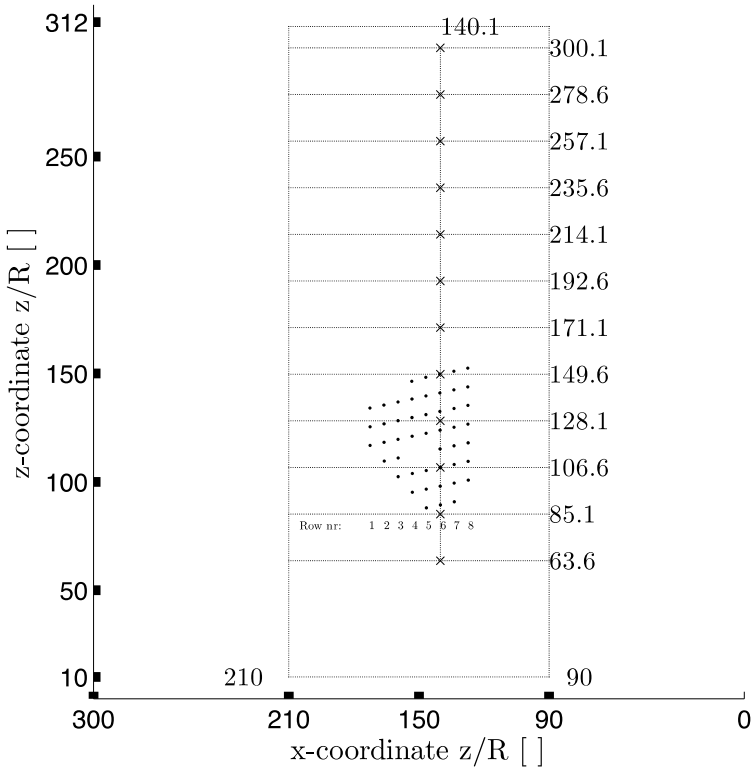

Figure 6-1 The placement of the turbines (•) in the domain covering 300 R * 322 R with the marked equidistant region of 120 R * 300 R. The flow is studied along the marked lines and for vertical profiles at the x's.

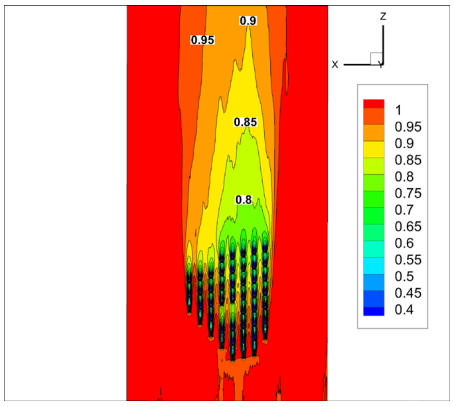

Figure 6-2 Streamwise velocity at hub height from the equidistant region in LES.

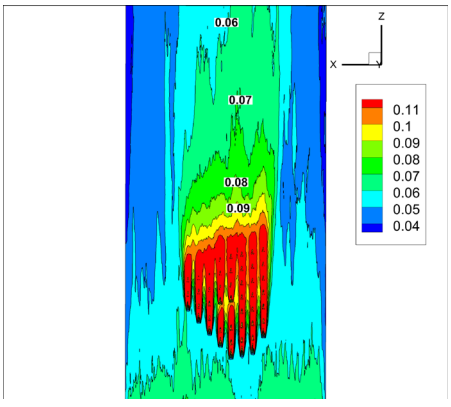

Figure 6-3 Horizontal turbulence intensity at hub height in LES.

In this study a comparison was also performed with WRF. The case was first run in WRF and the LES shear profile was chosen according to the profile in WRF. At the position of the first turbine in LES the turbulence level was the same as in WRF. Overall the relative production, Figure 6-4 , was overestimated in WRF and the recovery in the long distance wake was faster, see Figure 6-5.

The main reason was the resolution and how it impacts the turbine parametrization in WRF. Also the added turbulent kinetic energy (TKE), see Figure 6-6, was higher in WRF.

No site data for the wind speed in the long-distance wake was available for this wind farm, but comparing to Horns Rev the recovery using LES was in the correct order.

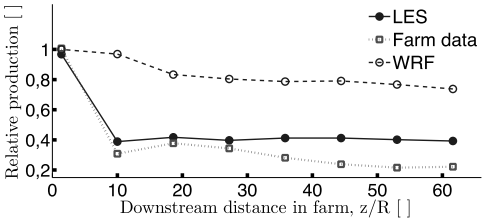

Figure 6-4 Relative production along Row 6.

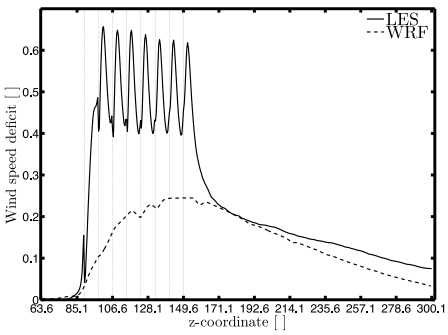

Figure 6-5 Streamwise velocity deficit (compared to z=63.8 R) for a line at hub height.

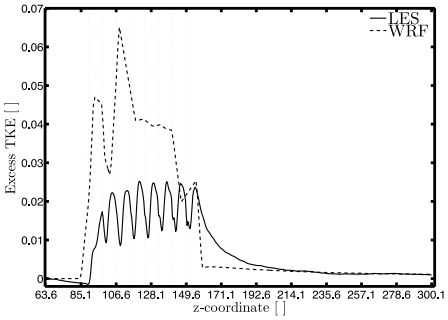

Figure 6-6 TKE (compared to z=63.8 R) for a) a line at hub height

6.1.2 Horns rev wind farm

To study how accurate the micro scale simulations model the wake also behind a wind farm a test case for Horns Rev (HR) is studied and compared to measurements from the site (Eriksson et al., 2012b). For the study only two rows of the farm were included in the grid, but with cyclic boundary conditions an infinite wind farm was simulated and the results were compared regarding the production and wind data at met towers 2 and 6 km behind the wind farm. The results show relatively good correlation between simulations and site data. However, a trend of increased production for the downstream rows and a faster velocity recovery at long distance was seen, compared to the site data.

In Eriksson et al., (2017) the full wind farm of Horns Rev I is simulated including the long distance wake up to 6 km downstream from the last turbine.

The wind farm is studied both in the mesoscale model WRF and in LES to be able to compare the two models. In this study site data is also available from measurements in the long distance wake. A comparison is also done to the results of the earlier study of HR using periodic BC. For the WRF simulation a similar

wind farm parameterization was used as for Lillgrund with the difference that no extra turbine induced turbulent kinetic energy was added and the resolution was higher. The layout of the wind farm is seen in Figure 6-7 which also give some details about the setup of the simulations. The result is Illustrated in Figure 6-8 for the velocity and in Figure 6-9 for the turbulence.

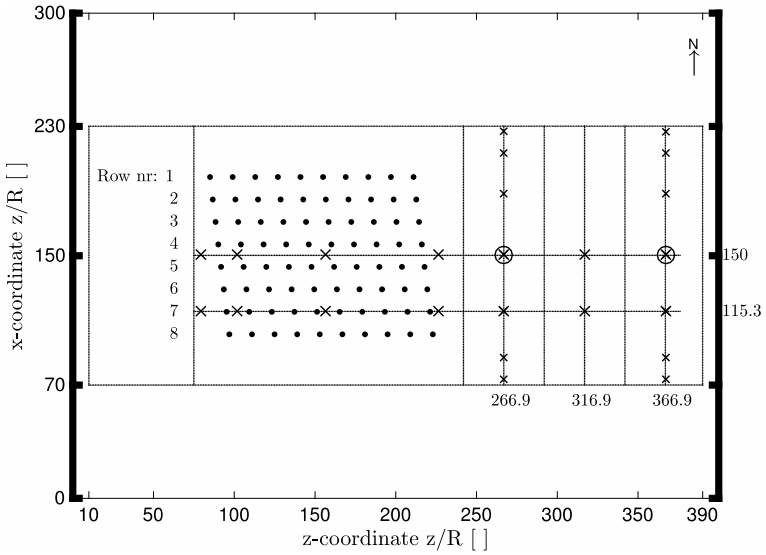

Figure 6-7 The placement of the turbines (•) in the domain covering 300 R * 400 R with the marked equidistant region of 160 R * 380 R. The flow is studied along the marked lines and for vertical profiles at the x's.

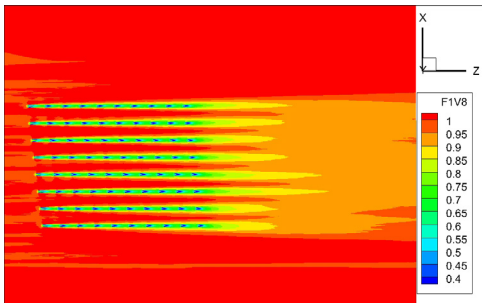

Figure 6-8 Streamwise velocity at hub height in LES, for the 270 deg case.

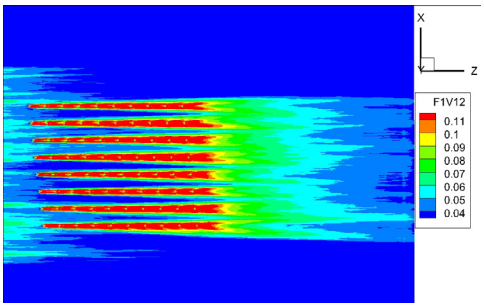

Figure 6-9 Streamwise turbulence intensity at hub height in LES, for the 270 deg case.

The relative production (Figure 6-10) in LES is lower for the first portion of the farm compared to the wind farm data but by the end of the wind farm the level is about the same. The values for WRF show, like the site data, a more gradual decrease with down stream distance but the level of relative production is underestimated. For the flow along row 7 inside the wind farm, seen in Figure 6-11 the horizontal velocity is in relatively close agreement between LES and WRF, but the more smoothed wake due to the lower resolution in WRF can still be noticed and WRF has a slightly lower velocity.

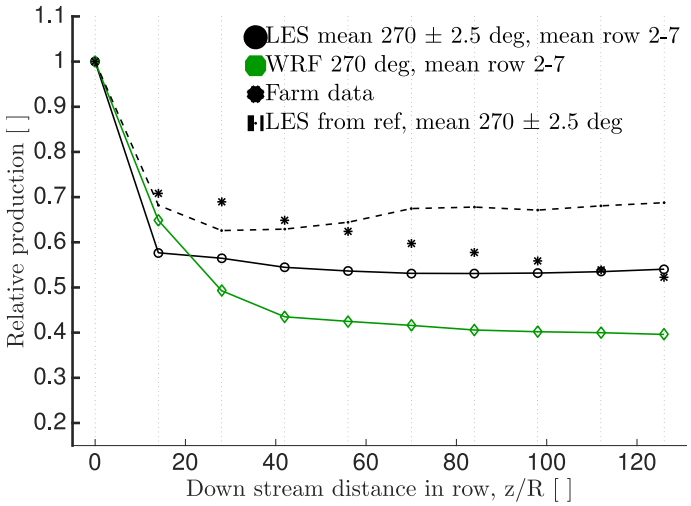

Figure 6-10 Mean of the relative production for the turbines in row 2-7 for LES, WRF and wind farm data. The older study using LES with periodic boundary conditions is included for comparison.

In Figure 6-11 also the flow along the mettowers is shown. The values for the mean of 270 ±2.5 deg in LES correspond to the met tower data. Behind the wind farm LES shows relatively good agreement with the met tower data for velocity, especially at 6 km. The long distance wake in WRF also shows relatively good agreement but has a slightly faster recovery.

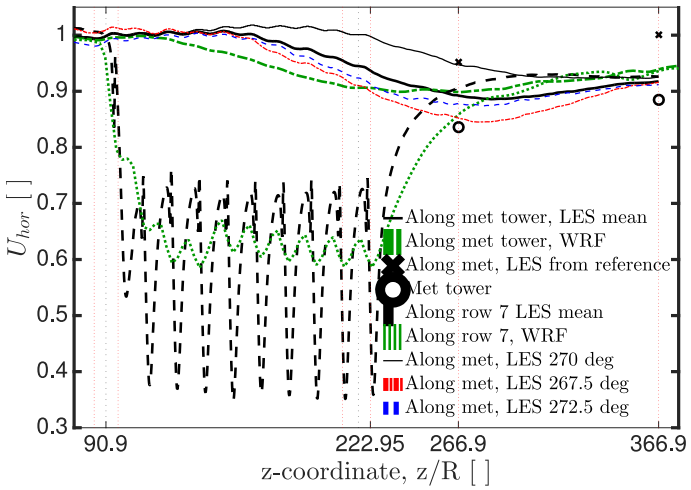

Figure 6-11 Normalized horizontal velocity (Uhor) in LES and WRF at hub height along the met towers and row 7. Site data and the older study (Eriksson et al., 2012b) using LES with periodic boundary conditions are included for comparison.

In Table 6-9 the values for the normalized velocity compared to the measuered values at the met towers are compared. To notice is the improvement from the first study of Horns Rev. It should also be noted that there are a number of uncertainties in comparison between the site data and the simulations, like direction uncertainties and non neutral stability conditions in the atmosphere.

Table 6-9 Normalized horizontal velocity (U_{hor}) at 2 km respectively 6 km behind the wind farm for LES, WRF, site data and results from the older study (Eriksson et al., 2012b) using LES with periodic boundary conditions. In brackets the difference in percentage compared to the site data is shown.

Distance	LES	WRF	Site data	LES old
2 km	0.89 (+5.9%)	0.9 (+7.1%)	0.84	0.95 (+13.1%)
6 km	0.92 (+3.7%)	0.94 (+5.6%)	0.89	1.0 (+12.6%)

6.2 FARM-FARM INTERACTION (MESOSCALE)

To study long-distance wind farms wakes and possible farm-farm interactions a WRF study was set up covering an area with 4 offshore wind farms in the outer Thames Estuary in the United Kingdom. The area of interest and the four wind farms included in the study, Gunfleet Sands, Kentish Flats, London Array, and Thanet are shown in Figure 6-12.

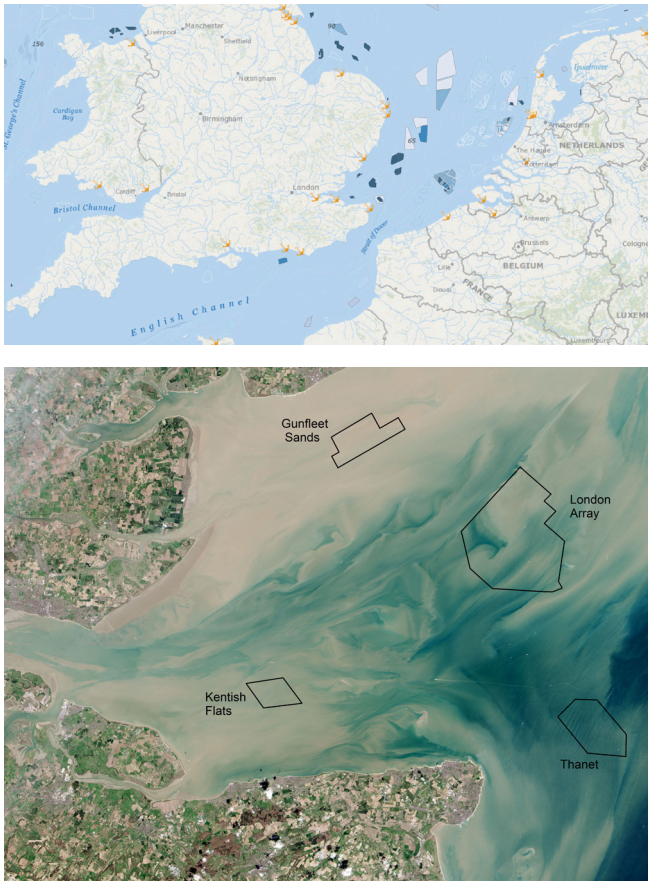

Figure 6-12. Location of the wind farms included in the study, Gunfleet Sands, Kentish Flats, London Array, and Thanet. Top panel from www.4coffshore.com; lower panel from https://en.wikipedia.org/wiki/London_Array#/media/File:Thames_Estuary_and_Wind_Farms_from_Space_NASA_with_annotations.jpg

A five-domain setup with two-way nesting was used. The parent domain had a horizontal resolution of 27000m and the innermost domain had a resolution of 333m. The turbine parameterization was active in the innermost domain only.

Three full months in 2016 were modelled, April, July, and October, allowing for a large range of different atmospheric stability cases. The model was run for 144 hours. Each model run was overlapping with 24 hours allowing for 24 hours spin up.

Initial and lateral boundary conditions were taken from the ERA Interim reanalysis provided by ECMWF (Dee et al. 2011). Spectral nudging was applied to the outer domain in order to constrain the model and to keep the model runs more consistent with the forcing data. Sea Surface Temperature (SST) and sea ice data was taken from OSTIA (Operational Sea Surface Temperature and Sea Ice Analysis, Donlon et al. 2012), a high-resolution daily analysis of the current SST at a resolution of 1/20° (approximately 5km).

To investigate possible production losses due to farm-farm interactions two cases were set up, one case with all four wind farms and one case without the London Array wind farm. The wind farm layouts for the two cases are illustrated in Figure 6-13.

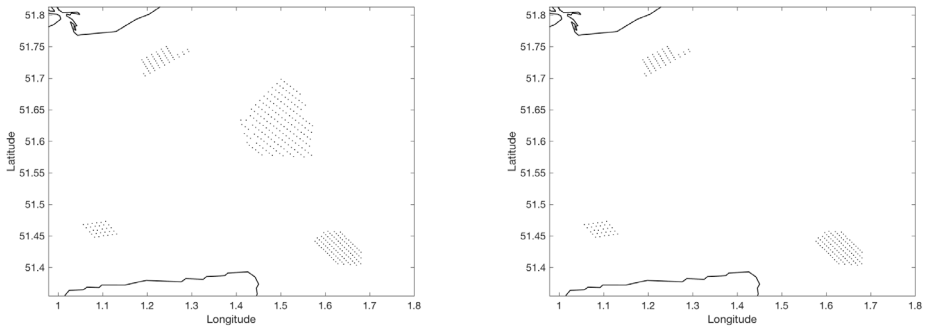

Figure 6-13. Wind farm layouts in the innermost nest with 333 m model grid resolution for the two cases, one with London Array and one without. Solid black lines are coastlines.

An example of modelled wind speed at 100m height in NNW wind direction is shown in Figure 6-14. In this case the effect of the London Array wind farm wake on the free stream flow for Thanet is noticeable.

Figure 6-15 further illustrates the effect of long-distance wind farm wakes, modelled wind speeds at 100m height when the wind turns slowly from nearly easterly flow to ESE flow over 5 hours. In the beginning of the period the Kentish Flats wind farm is in the wake from Thanet. As the flow turns with time the wake slowly turns and leave Kentish Flats in free stream flow conditions. Gunfleet Sands is partly in the wake of London Array in the beginning of the period and fully in the wake in the end of the period. The difference in free stream flow for Gunfleets Sands in the case with and without London Array is evident.

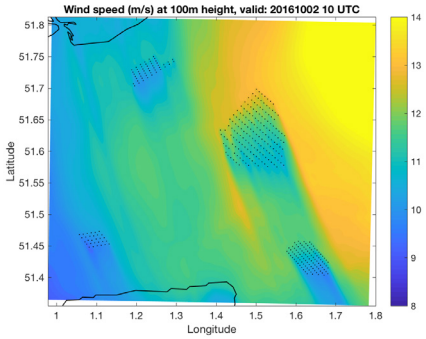

Figure 6-14. Example of wind speed at 100m height in a NNW wind direction. Solid black lines are coastlines.

During the three months simulated in the present study the effect of long-distance wind farm wakes is clear. The aggregated production losses over three months for Gunfleet Sands, Kentish Flats, and Thanet due to the London Array wind farm wake is presented in Table 6-10. The presence of London Array causes ~1.5% losses for Gunfleet Sands, ~0.5% losses for Kentish Flats and ~2% losses for Thanet. These numbers are large enough to motivate further studies of the effect of long-distance wind farm wakes in planned wind farm clusters.

Table 6-10. Aggregated losses in production due to the London Array wind farm wake.

Wind farm	Gunfleet Sands	Kentish Flats	Thanet
Loss (%)	1.59	0.52	1.98

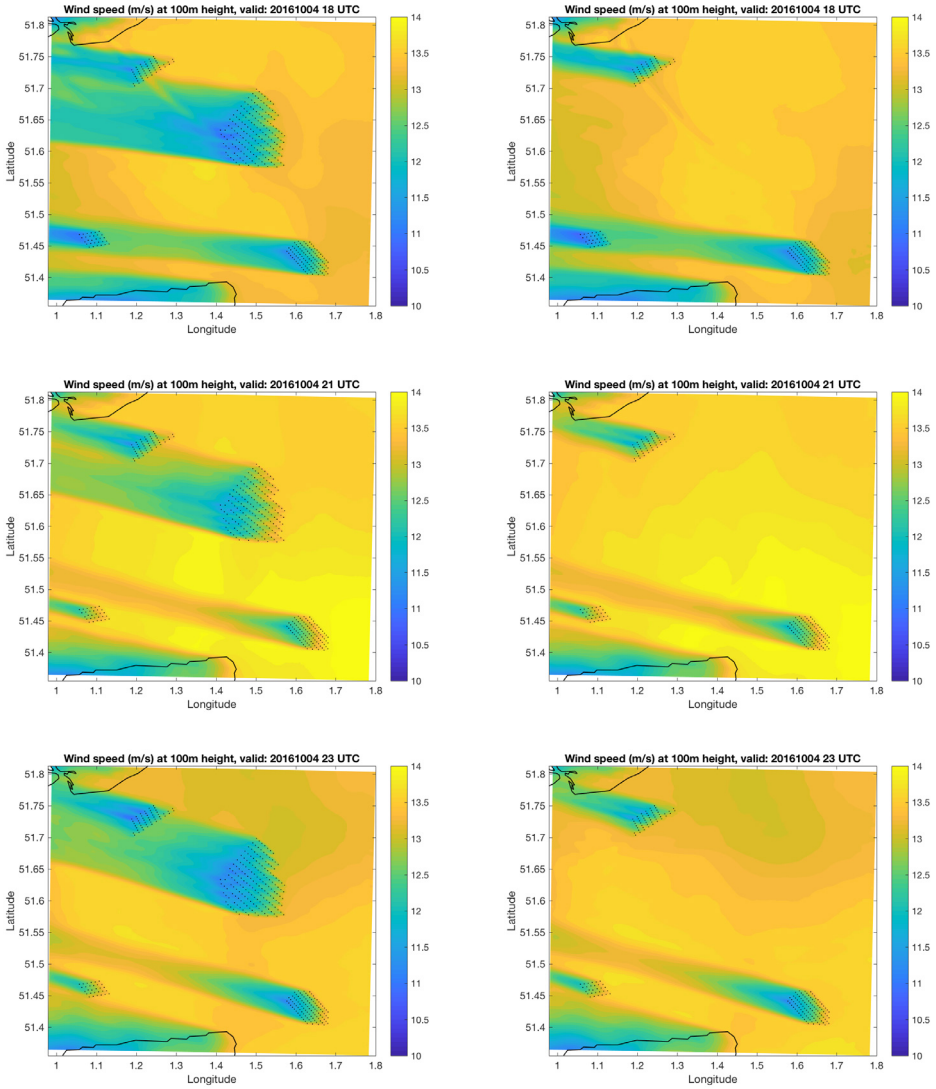

Figure 6-15. Examples of wind speed at 100m height when the wind turns from nearly easterly flow to ESE over 5 hours. Solid black lines are coastlines.

7 Conclusions and future work

- A microscale model is evaluated and developed

The microscale methodology has been verified to work with satisfactory accuracy within this and other studies. The challenge is that there remains a compromise between accuracy and required computational time. Today, we are able to perform accurate CFD simulations of individual turbines using actuator line (see section 1.1.2) methodology where coupling with load assessment is possible. We are also able to simulate the power production inside large wind farms using so called actuator disc methodology. For example, the farm simulations of Lillgrund shows excellent agreement with measurements.

In addition to what is possible there is a need to include load assessments with relatively "fast" LES simulations, i.e., actuator disc methods. This would allow us to study farm behavior, control and optimization of wind farms. Still, this would be to computational demanding methods for industry but by performing this type of simulation in research groups we can show the way and also use these simulations as verification to engineering models. Great steps forward in line with this has been made within this project but many challenges remains.

One should however remember that, for example, the Lillgrund simulation cases have been filtered for neutral atmospheric conditions and for that reason large future efforts remain to couple this methodology with tools to also include atmospheric stability. However, great achievements regarding farm simulations have been made within this project and this gives a solid foundation for future development.

- Farm wakes and mesoscale

For larger cases, as the simulation of entire wind farms and their long farm wake and possible a downstream farm, the needed computational time is still very challenging for LES. The mesoscale model WRF includes more meteorological parameters and is also less computational demanding (since it allows a coarser grid resolution) although a wind turbine parameterization is needed. Using LES we are instead able to simulate details in the wind farm (see comparison between LES and WRF in figure 5.10) but we have great challenges to scope over areas including two wind farms using this methodology. (The flow inside the wind farm will be better represented when using the finer grid in LES, due to the fact that the wake flow is better resolved.)

On the other hand the WRF methodology is able to include a large area and also include the atmospheric stability that on farm to farm scale will have a very large impact on the level of interaction between the farms. Therefore, we need capabilities from both methodologies to be able to fully model the physics.

An idealized farm to farm interaction case using microscale simulations (LES) is planned to be included in PhD thesis following up the Licentiate Thesis *Numerical Computations of Wakes Behind Wind Farms* (Eriksson, 2015) for micro scale simulations.

To summarize, the farm wake modeling have shown reasonable accuracy but also that the results are sensitive to the atmospheric stability and shows that when details are captured well with LES in relation to WRF, the atmospheric stability modeling is lacing.

Future work is therefore needed to couple these methodologies to be able to model details as well as atmospheric conditions in the future. This project has, however, made large steps in that direction.

8 Acknowledgment

Vattenfall is acknowledged for their contributions of data, participation in application process, meetings, thesis work etc. during the project. Especially we thank Jens Madsen, Jan-Åke Dahlberg, Jesper Nielsen Nissen and Ylva Odemark. Siemens is acknowledged for their contribution of Lillgrund data. The reference group including, besides partners, E.on, OX2 and the Energy Agency are highly appreciated for their contribution to meeting and project discussions.

DTU Wind Energy and KTH Mechanics are acknowledged for the contribution to the Nordic Consortium environment and fruitful discussions during consortium meetings. We would like to express a special thanks to Kurt Hansen at DTU Wind Energy for collaboration regarding filtering of data for the Lillgrund wind farm.

The simulations were mainly performed on resources provided by the Swedish National Infrastructure for Computing (SNIC) that are acknowledge for their support to the project.

We also would like to express our thanks to the Vindforsk program and the Swedish Energy Agency for their financial support of this project.

9 References

Betz, A. 1920 Das maximum der theoretisch möglichen ausnützung des windes durch windmotoren. Zeitschrift für das gesamte Turbinenwesen pp. 307–309.

Breton, S.-P., Nilsson, K., Olivares-Espinosa, H., Masson, C., Dufresne, L., Ivanell S. 2014 Study of the influence of imposed turbulence on the asymptotic wake deficit in a very long line of wind turbines. Renewable Energy 70 153-163

Churchfield, M. 2013 Generic siemens SWT-2.3-93 specifications. Tech. Rep. National Renewable Energy Laboratory.

Dee, D. P., Uppala, S. M., Simmons, A. J., Berrisford, P., Poli, P., Kobayashi, S., Andrae, U., Balmaseda, M. A., Balsamo, G., Bauer, P., Bechtold, P., Beljaars, A. C. M., van de Berg, L., Bidlot, J., Bormann, N., Delsol, C., Dragani, R., Fuentes, M., Geer, A. J., Haimberger, L., Healy, S. B., Hersbach, H., Hólm, E. V., Isaksen, L., Kållberg, P., Köhler, M., Matricardi, M., McNally, A. P., Monge-Sanz, B. M., Morcrette, J.-J., Park, B.-K., Peubey, C., de Rosnay, P., Tavolato, C., Thépaut, J.-N. and Vitart, F. 2011 The ERA-Interim reanalysis: configuration and performance of the data assimilation system. Q.J.R. Meteorol. Soc., 137: 553–597.

Donlon, C. J., Martin, M., Stark, J. D., Roberts-Jones, J., Fiedler E., Wimmer, W. 2011 The Operational Sea Surface Temperature and Sea Ice analysis (OSTIA). Remote Sensing of the Environment. doi: 10.1016/j.rse.2010.10.017 2011.

EMD. 2018. http://emd.dk/windpro/. Accessed: 2018-06-27.

Eriksson, O. 2015 Numerical Computations of Wakes Behind Wind Farms, Department of Earth Sciences Licentiate Thesis 2015, Uppsala universitet

Eriksson, O., Ivanell, S. 2012a, A Survey of available data and studies of Farm-Farm interaction, Proceedings of 8th PhD Seminar on Wind Energy in Europe, EAWE, Zürich, 2012, Proceeding-Presentation

Eriksson, O., Mikkelsen, R., Hansen, K. S., Nilsson, K., and Ivanell, S. 2012b Analysis of long distance wakes of Horns rev I using actuator disc approach. (J. Phys.: Conf. Ser. 555 012032)

Eriksson, O., K. Nilsson, K., Breton, S.-P., Ivanell, S. 2014 Analysis of long distance wakes behind a row of turbines -a parameter study, Journal of Physics: Conference Series 524 012152 (Torque 2014)

Eriksson, O., K. Nilsson, K., Breton, S.-P., Ivanell, S. 2015a Large-eddy simulations of wind farm production and long distance wakes. (J. Phys.: Conf. Ser. 625 012022),

Eriksson, O., Lindvall, J., Breton, S.-P., Ivanell S. 2015b Wake downstream of the Lillgrund wind farm - A Comparison between LES using the actuator disc method and a Wind farm Parametrization in WRF. (J. Phys.: Conf. Ser. 625 012028)

Eriksson, O., Baltscheffsky, M., Breton, S.-P., Söderberg, S. Ivanell, S. 2017 The Long distance wake behind Horns Rev I studied using large eddy simulations and a wind turbine parameterization in WRF, (J. Phys.: Conf. Ser. Wake 2017)

Fitch A.C., Olson J.B., Lundquist J.K., Dudhia J., Gupta A.K., Michalakes J., et al. 2012 Local and Mesoscale Impacts of Wind Farms as Parameterized in a Mesoscale NWP Model. Mon Wea Rev. Mar 6;140(9):3017–38. doi:http://dx.doi.org/10.1175/MWR-D-11-00352.1

Jonkman, J., Butterfield, S., Musial, W. & Scott, G. 2009 Definition of a 5-MW reference wind turbine for offshore system development. Tech. Rep. NREL/TP-500-38060. National Renewable Energy Laboratory.

Mann, J. 1994 The spatial structure of neutral atmospheric surface-layer turbulence. Journal of Fluid Mechanics 273, 141–168.

Mann, J. 1998 Wind field simulation. Probabilistic Engineering Mechanics 13, 269–282.

Michelsen, J. A. 1992 Basis3D - A Platform for Development of Multiblock PDE Solvers. Tech. Rep. AFM 92-05. Technical University of Denmark.

Michelsen, J. A. 1994 Block Structured Multigrid Solution of 2D and 3D Elliptic PDE's. Tech. Rep. AFM 94-06. Technical University of Denmark.

Mikkelsen, R. 2003 Actuator disc methods applied to wind turbines. PhD thesis, Technical University of Denmark.

NEWA. 2018. http://www.neweuropeanwindatlas.eu/. Accessed: 2018-06-27.

Nilsson, K., Breton, S.-P., Sørensen, J.N., Ivanell, S. 2014 Airfoil data sensitivity analysis for actuator disc simulations used in wind turbine applications. Journal of Physics: Conference series 524 012135

Nilsson, K., 2015. Numerical computations of wind turbine wakes and wake interaction. PhD Thesis, KTH Mechanics

Nilsson, K., Ivanell, S., Hansen, K.S., Mikkelsen, R., Sørensen, J.N., Breton, S.-P., Henningson, D. 2015a Large-eddy simulations of the Lillgrund wind farm. Wind Energy 18 449-467

Nilsson, K., Shen, W.Z., Sørensen, J.N., Breton, S.-P., Ivanell, S. 2015b Validation of the actuator line method using near wake measurements of the MEXICO rotor. Wind Energy 18 499-514

Nilsson, K., Breton, S.-P., Ivanell, S. 2015c Evaluation of the effects of using a power controller in LES/ACD simulations. Technical report

Réthoré, P.-E. 2009 Wind turbine wake in atmospheric turbulence. PhD thesis, AAlborg University.

Risø. 2018. http://www.wasp.dk/. Accessed: 2018-06-27.

Sarmast, S., Dadfar, R., Mikkelsen, R., Schlatter, P., Ivanell, S., Sørensen, J. & Henningson, D. 2014 Mutual inductance instability of the tip vortices behind a wind turbine. Journal of Fluid Mechanics 755, 705–731.

Skamarock, W.C., Klemp, J.B., Dudhia, J., Gill, D.O., Barker, D.M., Duda, M.G., Huang, X.-Y., Wang, W., Powers, J.G. 2008: *A Description of the Advanced Research WRF Version 3*. NCAR Technical Note NCAR/TN-475+STR, doi:10.5065/D68S4MVH.

Sørensen, N. N. 1995 General purpose flow solver applied to flow over hills. PhD thesis, Risø National Laboratory

Sørensen, J. & Myken, A. 1992 Unsteady actuator disc model for horizontal axis wind turbines. Journal of Wind Engineering and Industrial Aerodynamics 39, 139–149.

Troldborg, N., Sørensen, J., Mikkelsen, R. & Sørensen, N. 2014 A simple atmospheric boundary layer model applied to large eddy simulations of wind turbine wakes. Wind Energy 17, 657–669.

Vermeer, L. J., Sørensen, J. N. & Crespo, A. 2003 Wind turbine wake aerodynamics. Progress in Aerospace science 39, 467–510.

WindSim. 2018. http://www.windsim.com/. Accessed: 2018-06-27.

WIND TURBINE WAKES AND WIND FARM WAKES

Här har forskarna tagit fram beräkningar som gör det möjligt att optimera och styra en vindkraftspark med avseende på prestanda och last vilket innebär en minskad kostnad per producerad kilowattimme.

När ett vindkraftverk fångar vindens rörelseenergi skapas vakar, vilket innebär att vindhastigheten blir lägre och turbulensen ökar bakom kraftverket. När vindkraftverk placeras i grupper eller flera vindkraftparker ligger i närheten av varandra betyder det att produktionen minskar och lastpåverkan ökar jämfört med enstaka vindkraftverk.

Målet har varit att förbättra möjligheten att modellera vindkraftparker och interaktionen mellan olika parker. Att öka kunskapen om begränsningarna för olika simuleringsmetoder var ett ytterligare ett mål. Genom att uppskatta påverkan av vakar så kan man en mer optimal placering av vindkraftverk i grupper uppnås och driften bli mer optimal.

Data från vindkraftparken Lillgrund användes för utvärdering av lastpåverkan och data från vindkraftparkerna Lillgrund och Horns Rev användes för att jämföra simuleringsresultaten.

Energiforsk is the Swedish Energy Research Centre – an industrially owned body dedicated to meeting the common energy challenges faced by industries, authorities and society. Our vision is to be hub of Swedish energy research and our mission is to make the world of energy smarter! Vindforsk is operated in cooperation with the Swedish Energy Agency.

Energiforsk

Energimyndigheten